*Magnetic Resonance Imaging*, Vol. 3, pp. 173-208, 1985
Printed in the USA. All rights reserved.

0730-725X/85 $3.00 + .00


# • *Abstracts*

## ABSTRACTS OF PAPERS PRESENTED AT THE THIRD ANNUAL MEETING, SOCIETY FOR MAGNETIC RESONANCE IMAGING

### March 22-26, 1985, San Diego, California

MAGNETIC RESONANCE TOMOGRAPHY (MR-T) AT 3.4 MHZ FOR THE DIAGNOSIS OF INTRACRANIAL DISEASE IN CHILDREN

Francis W. Smith, Graham R. Cherryman, Thomas W. Redpath, Gordon A. Crosher and David L. Lloyd

Department of Nuclear Medicine, Aberdeen Royal Infirmary and Departments of Bio-Medical Physics and Bio-Engineering and Child Health, University of Aberdeen.

Using the Aberdeen 3.4 MHz Magnetic Resonance imager, over fifty children aged between 4 days and 16 years, have been examined. The Aberdeen imager is based on a 4 coil, air cored resistive magnet of 0.08 T and employs the "spin-warp" method of imaging. The pulse sequence employed consists of readout pulses every 1,000 msec with alternate readout pulses preceeded by inversion. The inversion is accomplished by adiabatic fast passage with a continuous delay which is normally 200 msec for routine imaging, but which may be varied from 50-450 msec.

With the development of small bore, specialised coils for the investigation of children's and neonatal heads, good resolution images of the brain are achieved. In the investigation of neonatal brain disorders, the routinely used, 200 msec Tau interval produces Inversion Recovery and calculated T1 images in which the long relaxation time of immature neonatal brain appears relatively featureless with no easy demonstration of developing white matter. The use of 300 and 400 msec T1 intervals provides better discrimination between grey and white matter and allows for easier demonstration of intra-cerebral haemorrhage, oedema and ischaemia.

The demonstration of supratentorial tumours is similar to conventional X-Ray CT, but differentiation of the tumour from any surrounding oedema may be difficult. However in the suprasella region, mid-brain, brain-stem and cerebellum MR-T is proving superior to X-Ray CT in the demonstration and diagnosis of tumour. Cranio-pharyngiomas have a characteristic appearance, having a cystic component of short relaxation time. One adenoma of the pituitary, confined to the gland and causing Cushing's syndrome was easily demonstrated. In two cases of hydrocephalus, in which X-Ray CT did not demonstrate any cause for the obstruction, MR-T demon-strated a 4 cm in diameter low grade astrocytoma of the pineal in one. In the other, a carcinoma of the choroid plexus which was obstructing the outflow of the fourth ventricle, the diffuse tumour was not clearly seen, having a T1 signal the same as normal cerebellartissue. Histologically this tumour appeared similar to renal cell carcinoma, one of the tumours which have a relatively short relaxation time. The use of intra-venous Gadolinium D.T.P.A. in a dose of 1 mmol/Kg body weight has been explored for the differentiation of brainstem tumour from haemorrhage. This paramagnetic contrast agent shortens the relaxation time in tumours but we believe that the use of a higher dose, in the region of 2.5 mmol/Kg would be more appropriate.

The use of MR-T for the investigation of the neonatal and child's brain has many advantages, not the least of which is its lack of ionising radiation which enables it to be used for the regular follow-up of hydrocephalus following shunting and routine examination of suspected intracranial disease.

INTRACRANIAL MASS LESIONS OF CHILDREN VIA MAGNETIC RESONANCE IMAGING (MRI) AT 0.27T.

P.D. Lester, W.S. Yamanashi, R.E. Woosley
City of Faith Medical and Research Center, Tulsa, OK

and

P.D. Barnes
Children's Memorial Hospital, Oklahoma City, OK

Congenital or acquired cystic and solid masses of intracranium, when suspected clinically, usually present no difficulty in imaging localization by existing means (plain films, CT, isotopic imaging and angiography). Often, all of these modalities are utilized in obtaining pretreatment information for etiology, tissue characteristics, mass localization and tumor extent. The objective of this study is to answer occasionally raised questions concerning the true extent of disease, involvement of vital contiguous structures and adequacy of soft tissue visualization at the base of the brain and upper cervical cord.

Twenty-two children with masses due to congenital, cystic, or vascular etiologies or acquired neoplastic or inflammatory lesions were MR scanned. The imager used was a Picker MR VISTA 2055 with a 0.5T max. superconducting

magnet operated at 0.27T. The imaging method was 2DFT with multiple slicing, with slice thickness 0.7cm, pixel matrix 256 x 256, number of image averaged 2 were used. Spin-echo (SE) sequence with TE/TR (both in ms) of 60/2000 and 120/2200 were most frequently used.

Based on this work and other MRI intracranial studies, we conclude that (1) Initial screening examination for suspected intracranial mass lesion should be MRI; (2) MRI is equal or superior to existing modalities in (a) tissue characterization, (b) mass extent and involvement of contiguous structures and (c) pretreatment localization; (3) Contrast enhanced CT or angiography is required in suspected vascular malformations and may be needed to determine the vascular nature of some intracranial neoplasms; (4) Multislice multiplanar evaluation of children provides a nonhazardous technique for evaluating the entire upper neural axis for primary masses and secondary lesions.

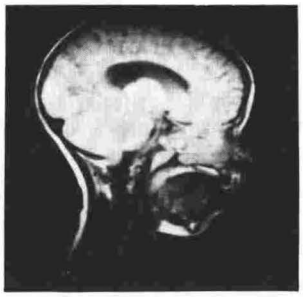

## MAGNETIC RESONANCE IMAGING IN CHILDREN WITH DISSEMINATED ENCEPHALOMYELITIS

Val D. Dunn,M.D., Zack Perdue,M.D., James F. Bale, Jr.,M.D., William E. Bell,M.D., & James C. Ehrhardt,Ph.D.

Departments of Radiology, Neurology, and Pediatrics, University of Iowa Hospitals & Clinics, Iowa City, Iowa

Disseminated encephalomyelitis, an uncommon disorder of central nervous system white matter, typically occurs following childhood viral infections. Although CT may demonstrate white matter lesions, many children have normal CT studies inspite of widespread neurologic abnormalities. We report two children with disseminated encephalomyelitis who were studied using magnetic resonance imaging (MRI). Case 1, a 7-year-old girl, had recurrent signs characterized by diplopia, headache, ataxia, hemiparesis, and long tract signs. Case 2, a 5-year-old girl, had a three month illness with alternating hemiparesis, optic neuritis, focal seizures, and ataxia. CT studies showed poorly demarcated white matter lesions. MRI in both children demonstrated multifocal white matter lesions of cerebrum and cerebellum which corresponded to clinical signs. Studies to exclude other conditions associated with central nervous system demyelination were negative. Both children improved rapidly with corticosteroid therapy. MRI in Case 1 showed progressive resolution of white matter lesions in conjunction with clinical recovery. These observations indicate that MRI has diagnostic utility in children with possible disseminated encephalomyelitis.

The pattern of involvement on MR imaging in both cases was very similar and is likely to be characteristic of this disorder. Although experience is still small, it appears that MRI may become the imaging method of choice in disseminated encephalomyelitis as it is in multiple sclerosis. Interestingly, the constellation of clinical symptoms and signs in disseminated encephalomyelitis resembles that seen in acute multiple sclerosis as well as viral encephalitis or toxic encephalopathy. Both conditions have multifocal white matter lesions but those of disseminated encephalomyelitis tend to involve larger areas, are more poorly defined, and are not as likely to be periventricular as those seen in MS. The lesions and symptoms of disseminated encephalomyelitis may resolve in a matter of weeks with treatment.

## EVOLUTION OF CEREBRAL INFARCTION: MRI APPEARANCE WITH PATHOPHYSIOLOGICAL CORRELATION

Bonnie D. Flannigan, M.D., William G. Bradley, M.D., Ph.D., and Keith E. Kortman, M.D.

Glendale Adventist Medical Center, 1509 Wilson Terrace, Glendale, CA 91206
NMR Imaging Laboratory, Huntington Medical Research Institutes, Pasadena, CA 91105

Forty patients with cerebral infarction of varying stages (acute, subacute, and chronic) were studied with a .35T and .5T MR imager using spin echo pulsing sequences. The age of each infarct was determined by clinical history and CT appearance. The MR images were compared to known time-related microscopic pathological changes of cerebral infarction.

Distinct MR patterns were identified during the evolution of cerebral infarction. Acute and subacute infarction is characterized by sharply marginated areas of high intensity on T2 weighted images. This is felt to represent central vasogenic edema confined centrally by peripherally swollen cells due to cytotoxic edema. Chronic infarcts had two distinct appearances. One type had a two zoned appearance; a central area of low intensity corresponding to macrocystic encephalomalacia, and a peripheral zone of higher intensity corresponding to the surrounding gliotic zone with microcysts. The higher intensity zone represents hydration layer water with a relatively short T1 and long T2. The lower intensity zone was similar in intensity to CSF and represents bulk phase water with a much longer T1 relaxation time.

The second type of chronic infarction appeared as an area of CSF intensity without surrounding high intensity. These infarcts are felt to have relatively little gliosis or gliosis without microcyst formation.

## CRANIOPHARYNGIOMA: CORRELATION OF HIGH RESOLUTION CT AND MRI

Ann C. Price, M.D.; Val Runge, M.D.; Joseph H. Allen, M.D.; Robert M. Kessler, M.D.; Martin Sandler, M.D.; C. Leon Partain, M.D.

Vanderbilt Univ. Med. Ctr.; Dept. of Radiology & Radiological Sciences; Nashville, TN 37232; (615) 322-3747

Twelve patients with surgically proven Craniopharyngiomas were evaluated with a GE CT/T 8800 scanner in the standard axial plane (pre and post contrast) and either as a direct coronal study or sagittal/coronal reformatted images from 1.5 mm axial sections. Eight of these patients were examined with MRI at 0.5 tesla (Technicare) utilizing multiple sequences to encompass both T1 and T2 characteristics of the lesion.

The CT changes of cyst formation, loculation, calcification and rim and nidus enhancement are compared to MRI changes. The T2 weighted (SE 120/1000) sequence showed a bright signal intensity increase which was superior to CT in defining the suprasellar extent, loculation, post-surgical recurrences, and relationship of the tumor to the sella and pituitary.

In a previously reported study of 50 pituitary abnormalities, increase in signal intensity occured in Craniopharyngiomas and previously irradiated pituitary tumors. Other causes of signal intensity increase include empty sella (reported) and lipoma (theoretical). This has application in differential diagnoses for those tumors that do not have specific characteristics at CT and in the small intrasellar tumor that simulate the appearance of a prolactinoma.

Despite the assets offered by MRI, the cystic nature, calcification and features of the smaller intrasellar tumors remains better defined by CT. Until slice widths can be made narrower, CT will retain its premier role as the initial diagnostic modality.

## MAGNETIC RESONANCE IMAGING OF THE HUMAN CORPUS CALLOSUM IN RELATION TO GENDER AND HANDEDNESS

Carolyn Ely Coffman, M.D., Val D. Dunn, M.D., Paul J. Eslinger, Ph.D., Henry A. Nasrallah, M.D., Antonio J. Damasio, M.D.

The University of Iowa, Depts. of Neurology, Radiology and Psychiatry, Iowa City, Iowa

Forty volunteers (10 male and 10 female right handers and 10 male and 10 female left handers) had Magnetic Resonance (MR) scans of the brain done in the midline sagittal plane. The MR images were used for measurements of the corpus callosum in the four subgroups. Autopsy studies have produced preliminary evidence that sexual dimorphism and right/left differences exist in the corpus callosum. MR is the first imaging modality which allows for the visualization and accurate measurement of midline sagittal structures in the intact human brain.

In vivo measurements, from MR scans, supported previous data by showing important structural differences between right and left handers. The corpora of male and female left handers were similar, but those of male and female right handers revealed striking sexual dimorphism. These data provide powerful evidence of different brain organization in relation to gender and cerebral dominance.

## DESIGN BASICS FOR DEDICATED MR RECEIVER RESONATORS

Neil T. Wolfman, MD, Rodney K. Williams, MS, Ben E. Wall, BS and Paul R. Moran, PhD

Bowman Gray School of Medicine, Wake Forest University

For special purpose medical studies, dedicated MR resonators offer the advantages of very high specific sensitivity, minimization of MR image artifact from erratic motions of organ systems outside the desired field of interest in the human anatomy, achievement of the optimum reception condition of patient-loading dominance, reduction of thermal noise sources to origins limited by the MR volume desired, and availability of system advantages

offered by "crossed-coil" separate exciter and receiver circuits. Basic design considerations involve rather simple and fundamental considerations of highest deliverable signal-power from a receiver resonator and the sources of patient-dominated coil dissipation. This was applied successfully in a recently published triple-coil resonator for mammographic MRI, and further elaboration much improves reception uniformity while achieving even higher specific sensitivity. "Folded resonator" concepts also have been applied with success, which exploit the concept of resonator orthogonality as a generalization of the crossed-coil perpendicularity operation. Neck, knee-joint, small animal, and spinal-cord versions have been designed, built, and tested; the resonator structures and results from each are demonstrated in actual scans for a 1500G MRI unit.

## AN EFFICIENT, HIGHLY HOMOGENEOUS RF COIL FOR WHOLE BODY IMAGING AT 1.5T

C.E. Hayes*, W.A. Edelstein**, J.F. Schenck**, O.M. Mueller**, and M.G. Eash*

*G.E. Medical Systems, Milwaukee, WI **G.E. Corporate Research & Development Center, Schenectady, NY

We have developed rf coils for high field head and whole body imaging which achieve near optimal signal sensitivity and $B_1$ field homogeneity. The design, based on a cylindrically symmetric slow wave structure, has a number of advantages. The high sensitivity permits one to obtain, as expected, the nearly linear increase in signal-to-noise as a function of frequency or static magnetic field [1]. The improved rf field homogeneity is needed to acquire accurate multi-echo pulse sequences. The cylindrical symmetry allows quadrature drive and reception which, in turn, decreases rf power requirements by a factor of two and increases signal-to-noise by a factor of $\sqrt{2}$ [2].

Hoult and Lauterbur [1] have pointed out that magnetically induced sample losses can (and should) become the dominant noise source as the imaging frequency (or static field $B_0$) is increased. Hence the optimum signal-to-noise ratio for a given frequency and coil geometry occurs when the rf coil losses are negligible compared to the sample losses. Coil design factors such as the filling factor, coil quality factor Q, and coil efficiency all contribute to coil sensitivity but none is paramount. The best measure of rf coil sensitivity is the ratio of the Q for the empty coil and the Q for the coil loaded by the patient. For our coils, this ratio $Q_{empty}/Q_{loaded}$ is typically greater than five. This implies that the rf coil losses contributes less than 11% of the noise voltage.

The use of a superconductive magnet requires a transverse rf field within a cylindrical volume. A perfectly homogeneous transverse magnetic field in an infinitely long cylinder can be produced by surface currents which run along the length of cylinder and are proportional to $\sin\theta$, where $\theta$ is the polar coordinate angle. Our coil design approximates the ideal current distribution in a structure with discrete parallel conducting paths. The chief cause of $B_1$ inhomogeneity is the unavoidable rolloff of field intensity at the ends of the coil. A long coil produces more uniform sensitivity for coronal and sagittal imaging. A short coil is more favorable for axial imaging since it picks up less noise from portions of the body outside the imaging plane. Hence, a tradeoff is required when choosing coil length. Experimental observations verified the expected improvement in $B_1$ homogeneity for our new design compared to saddle coils and slotted tube resonators.

The high order of axial symmetry of the new design permits use of two transmit drive points and two receive points located $90^0$ apart. By proper phasing of the two transmitted signals, a circularly polarized rf field results which reduces the required power by a factor of two. Likewise, by the proper combination of the two received signals, the signal-to-noise is enhanced by the factor of $\sqrt{2}$ [2]. Both improvements have been observed [3].

1. D.I. Hoult and P.C. Lauterbur, J. Magn. Reson. 34, 425 (1979).
2. C.-N. Chen, D.I. Hoult, and V.J. Sank, J. Magn. Reson. 54, 324 (1983).
3. G.H. Glover, C.E. Hayes, W.A. Edelstein, O.M. Mueller, H.R. Hart, C.J. Hardy, M. O'Donnell, and W.D. Barber, Third Annual Meeting, Society of Magnetic Resonance in Medicine, p. 264 (1984).

## DESIGN, CHARACTERIZATION, AND EVALUATION OF WHOLE BODY RESONATORS FOR 1.5T PROTON IMAGING

George J. Misic, John L. Patrick, Aarne Lillo and Robert W. Brown(*)

Picker International, 5500 Avion Park Drive, Highland Heights, Ohio 44143
(*) Case Western Reserve University, Cleveland, Ohio 44106

The difficulties encountered in the construction of R.F. coils for head imaging at 64 MHz and beyond are compounded when whole body imaging is desired. Patient access considerations significantly restrict the physical geometry of the probe structure. The region of good field homogeneity must be expanded along all three axes to provide a useful field of view. Finally, it is advantageous to develop a structure that allows a head resonator to be used for head imaging without removing the body resonator structure from the NMR system.

Two coil designs were developed to address the problems of body imaging. The first was designed for maximum patient access. It has an overall diameter of 60 cm, providing a very large patient aperture. This resonator has a mechanical length of 60 cm and an electrical length of $\lambda/2$. It is a balanced

structure designed for very high unloaded "Q" and excellent field homogeneity in all three imaging planes over a 45 cm field of view.

The second design was formed as an elliptical structure having a major axis of 55 cm, a minor axis of 39 cm, and a length of 60 cm. This geometry results in an optimized filling factor with a patient of normal size. It is also a balanced $\lambda/2$ configuration, possessing excellent field homogeneity along with a high unloaded "Q".

The design considerations of each resonator are presented, along with methods of tuning and matching to a 50 ohm unbalanced transmission line. The performance of each design as a single probe for transmission and reception is discussed. Details of a probe multiplexing scheme for interfacing to the spectrometer are revealed. Techniques to allow crossed coil operation or independent decoupled operation with a head resonator are also discussed.

The probes were evaluated for both electrical performance and image quality under actual scan conditions. The merits and shortcomings of each device are compared with theoretical calculations and discussed.

## AN INTERACTIVE ARRAY PROCESSOR (IAP) FOR MULTI-DIMENSIONAL MR IMAGING

S.D. Mirer, M.J. Hennessy, L.E. Tanski, K.E. Mathews, D.M. Butler

Intermagnetics General Corporation, MRI Laboratory, Troy, NY

Software is a critical component of MR imaging, not only as part of an imaging system, but also as a tool in its development. The software must not only be capable of controlling the entire imaging process, but should provide tools for developing new algorithms and techniques and for debugging the entire hardware/software system. So that scientists and engineers can concentrate on higher level problems without distraction, the software should be easy to use, relieving typical users from trivial programming details. To meet all of these requirements, we have developed an Interactive Array Processor (IAP).

The central data structure in MR imaging is the array, from simple one dimensional FIDs to three or four dimensional chemical shift images. IAP commands operate directly on arrays, eliminating programming complications introduced by more primitive languages. IAP also supports external hardware and graphics displays, providing the functionality necessary for multi-dimensional MR imaging. IAP is implemented on a VAX-11/750 under VMS using Fortran-77.

Experience with IAP and its predecessor, the Interactive Vector Processor (IVP), supports our design approach. In a research environment whose computational demands include not just the main application but general signal processing and a variety of mathematical problems, both IVP and IAP have proven to be highly effective and far superior to the traditional Fortran and assembly language approach.

## RF POWER PROCESSING FOR MRI

O. Mueller, W. A. Edelstein and D. Vatis

General Electric Corporate Research and Development Center, P.O. Box 8, Schenectady, NY 12301

A higher field strength in a magnetic resonance imaging/spectroscopy system requires more RF power. Interesting problems occur in the processing of many kilowatts of MR frequencies, the subject of this paper.

A solid-state RF power amplifier for the 50-70 MHz MR frequency band (1.5 Tesla) has been designed, built and demonstrated which generates 5-6 kilowatts with only 4 new MOS field-effect transistors at a supply voltage of 60-70 volt. High DC-voltages in the kilovolt range required for tube PA's have therefore been eliminated. Much larger bandwidth can be obtained compared to vacuum tube power amplifiers due to the successful implementation of transmission line impedance transformers. The latter have been constructed with coaxial tubes of low characteristic impedance which have been placed through several ferrite beads.

An instantaneous full-power bandwidth of more than 20 MHz (F=50-70 MHz) has been demonstrated. An even wider frequency band is safely obtained at reduced power levels without any retuning or circuit change. The center frequency of the PA can easily be moved to another value, for example 35 MHz (0.8 Tesla) by slightly changing 4 strip-line inductors of the transistor input matching network. Linearity performance and protection circuits will also be discussed. The pulse power is delivered by a large capacitor bank (0.4 millifarad) so that relatively small power supplies can be used. Tube and solid-state power amplifiers, their advantages and drawbacks, are compared with each other.

Two- and four-way high-power combining and splitting hybrids made from transmission lines have been built. A push-pull combiner circuit can be used to improve the linearity performance of four PA-modules. Design formulas and performance data are presented for 90° quadrature hybrids built with transmission lines or lumped elements. They are necessary for the generation of rotating RF fields. High-power BALUNs (Balance-unbalance transformers) have also been designed.

## ULTRA HIGH RESOLUTION MRI FOR SMALL ANIMAL MODELS

G. Allan Johnson, Ph.D.[1], Sally Gewalt, M.S.[1], Morrow B. Thompson, Ph.D., D.V.M.[2]

[1]Duke University Medical Center, Durham, North Carolina 27710
[2]National Institute of Environmental Health Science, Research Triangle Park, North Carolina

Initial MRI studies in small animals showed the great sensitivity of the technique. However, the specificity was less than early workers hoped. If MRI is to attain its potential, small animal models must be understood. With these models, one can produce well-characterized disease, definitive histopathologic correlation, and an adequate statistical sampling. These studies can provide the basis for applying MRI in human disease.

Unfortunately, instrumental requirements have limited the use of MRI in small animals. The smaller structures require substantially higher resolution. Generally, higher resolution (smaller pixels) requires increased signal-to-noise in the imaging system.

By appropriate modification of a prototype 1.5T system for humans, this group has obtained images with pixels of 50 x 50 microns in a 1 mm thick slice. Modifications include a smaller (22.5 cm) gradient coil which can be driven to supply gradients > 3 gauss/cm. Rf coils for small animals have been built which provide an improvement of 50X in SNR over that of a human head coil.

Using this apparatus, images have been obtained in several small animals. In the rat, microvascular structures in the kidneys and liver have been demonstrated. In the coronal plane, the renal vessels, adrenal glands and vasculature, and ureters have been clearly seen. Images of the rat brain obtained with a 2 cm field-of-view demonstrate the ventricles well.

Quantitative T1 and T2 measurements have been performed on chemically induced liver tumors in the rat. These results in MRI microscopy open an entirely new field of research.

## A MULTI-PURPOSE RAT PROBE FOR IN-VIVO SPECTROSCOPY

M. J. Hennessy, J. J. Gramm, B. E. Hammer

Intermagnetics General Corporation, MRI Laboratory, Troy, NY

A multi-purpose probe has developed for in-vivo studies of rats and small animals in an Intermagnetics IGC 2.1T superconducting magnet system. The probe consists of a large saddle-shaped transmitting coil and a small surface coil for localization. This combination gives good RF homogeneity and sensitivity. Provisions were made for containing and positioning the rat during the experiment. The probe has proven to be very stable under heavy laboratory use.

## AN EFFICIENT, LOW-COST NMR IMAGING MACHINE

Luc DARRASSE, Hervé SAINT-JALMES, Michel SAUZADE
Institut d'Electronique Fondamentale - Bâtiment 220 Université Paris 91405 Orsay Cedex (F)

We present an home-built NMR machine incorporating original technical solutions for optimum efficiency. It has produced so far good quality 0.1 Tesla head images.

The system design is based on simple modules :

- a four coil resistive magnet provides 20 ppm homogeneity over a 250 mm sphere.
- a home-built gradient system [1] produces up to 5 mT/m with 2% linearity.A 2 ms rise time (to 0.1% flatness) is achieved with only 350 W of switching power.
- separate emitting and receiving coils allow closer matching to the size of imaging volume (e.g. from the whole body to the eye).
- an original Mosfet rf emitter [2] delivers up to 1.5 kW rms at 4.25 MHz.
- our wide-band (800 kHz) quadrature homodyne receiver features only two tunable circuits.
- real-time control of all modules is achieved with two identical LSI timing boards [3] featuring a total of 20 independently programmable timers. In a first step of technical development, we use this logic hardware to directly drive the gradients and rf emitter (i.e. no pulse shaping).
- the computer system is a DEC LSI 11/23 with two CDA array processors for FFT computing and image display.

Our design allows easy implementation of existing and future imaging methods (projection - reconstruction, 2D and 3D, etc ...). Moreover the system is reliable and low-cost (we spent less than $200,000 for buying or subcontracting equipment) mainly due to the low field and the correspondingly very low gradient switching power.

The good quality of our results (see right) suggest that low-field MRI machines may offer an interesting cost-performance ratio for routine diagnosis in a standard hospital environment.

References

1. H. Saint-Jalmes, J. Taquin, Y. Barjhoux
to appear in Magn. Reson. Med. (1985).
2. L. Darrasse, Rev. Sci. Instrum., 53, 1561 (1982)
3. H. Saint-Jalmes, Y. Barjhoux
Rev. Sci. Instrum. 53, 1 (1982).

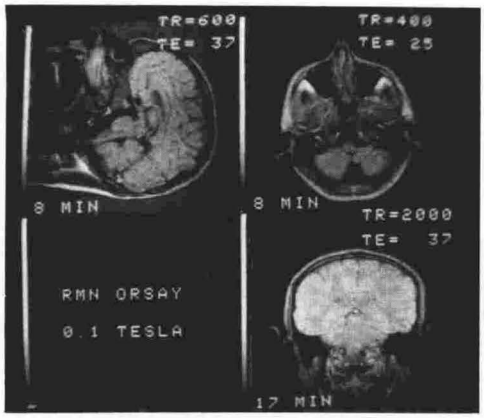


128x128 2D FT images.1cm slice thickness
10 kHz bandwidth when TE = 25 ms
5 kHz bandwidth when TE = 37 ms

FIELD FOCUSED INTERSTITIAL HYPERTHERMIA AND MAGNETIC RESONANCE (MR) TOMOGRAPHY PERFORMED WITH A COMMERCIAL MR SCANNER AND AN INVASIVE GROUNDED PROBE IN PHANTOMS AND IN RAT TISSUES.

W.S. Yamanashi, M.R. Fesen, D.W. Anderson, P.D. Lester
City of Faith Medical and Research Center, Tulsa, OK 74137
and
J.W. Frazer, C. Jones
M.D. Anderson Hospital, Houston, TX 77030

Facilitating a MR scanner in a (1) diagnostic as well as (2) therapeutic modalities was demonstrated. In the diagnostic mode, a Picker MR VISTA 2055 scanner with 0.255T field strength, 10.86 MHz resonance frequency was operated in a conventional manner i.e., 2DFT imaging, multislicing, SE pulse sequence with TE = 40 ms, TR = 1000 ms. In the therapeutic mode, the scanner was used as an RF power source and the grounded probe as an eddy current convergence device to produce hyperthermia in phantoms and tissues (Figure 1). The grounded hyperthermia probe[1,2] consisted of a electrically conducting nonferromagnetic needle partly sheathed with an insolator (Teflon), the conducting portion is designed to be inserted into the tumor, whereas the insulated portion penatrates volume between skin surface and the tumor. The other end of the probe was grounded via a tuning device. The tuning devise is a series variable inductor and capacitor whose resonance characteristics and transfer functions were analyzed with a Hewlett Packard HP-3577A network analyzer with a HP-3567 S-parameter ports ($S_{11}$, $S_{12}$, $S_{21}$, $S_{22}$). The RF transmitter, amplifier and the body coil of the scanner was tuned with the load (phantom and ground probe) and driven at 2% duty cycle without digital control. Gradient pulses were not used in this mode. The heating curves obtained with this extremely low duty cycle setting are shown in Figure 2, implying high efficiency of the grounded probe method. Monitoring of the heating rate was done with a fluoroptic thermal probe (Luxtron 1000-B), heating isotherms in phantoms were approximated with liquid crystal sheets. A nonferromagnetic metal was used for the hyperthermic probe. The length of the conducting tip can be used to approximate the radius of the hot spot up to r=3.5 cm, above this length, the hot spot becomes elipsoidal. Our previous experience with ground elements showed that larger phantom volume (15 cm diameter, 16 cm height), can be heated evenly by the use of one grounded probe and two switched grounded pads[2].

In order to obtain maximum temperature typically used for regional hyperthermia 42°C - 57°C, the amplifier should be operated at higher % duty cycle, this can be done when an appropriate permit is given by the government for the combined modality protocol.

[1]Boddie, AW; Yamanashi, WS; Frazer, JW; et al Med. Instr. 17 358-365 (1983).
[2]Yamanashi, WS; Boddie, AW; Frazer, JW; et al Med. Instr. 18 220-223 (1984).

Yamanashi et al continued

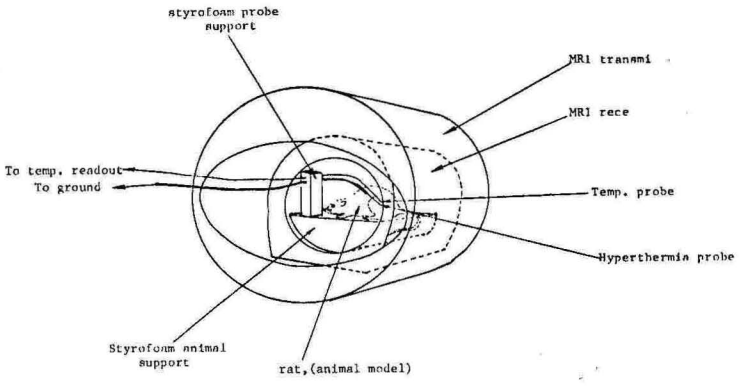


Figure 1
The experimental setting of the field focused interstitial hyperthermia performed with a tuned grounded probe and a commercial MRI scanner. The heating rate was monitored with a fluoroptic probe, the grounded probe was used as an eddy current convergence device to produce hyperthermia. The thermal probe tip was placed in the vacinity (2-3mm) of the tip the grounded hyperthermia probe. Control data was obtained without application of RF power to the MRI coil.

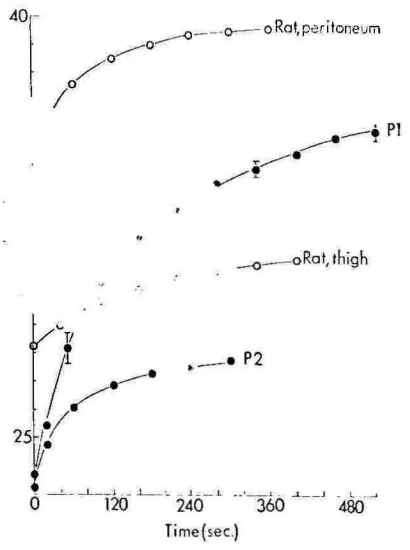


Figure 2
Heating curves obtained using the setting shown in Fig. 1. MRI transmitter was operated at 2% duty cycle. (RF pulse width 900 micro sec., pulse interval 50ms). from the top: rat peritoneum, Phantom-1 (apple), rat thigh muscle, and phantom-2, (gellatin).

IMAGING OF OIL EXPULSION FLOW BY WATER IN RESERVOR CORES WITH SOLENOID COILS USED IN A 0.25T MRI SCANNER.

B.A. Baldwin
Phillips Petroleum Co., Bartlesville, OK 74004 and W.S. Yamanashi and P.D. Lester
City of Faith Medical and Research Center, Tulsa, OK 74137

For a considerable time the petroleum industry has used average oil and water saturations of core plugs to determine the amount of oil originally in place and produced by a specific production process. However, it has not been possible to spatially locate these two fluid components in the reservoir rock. Simple mathematical and experimental models can be used to predict that water flow through a reservoir will occur either in a heterogenious fashion, leaving macroscopic volumes of oil surrounded by water or in a homogeneous fashion, leaving oil as microscopic globules inside individual pores. A Picker model MR VISTA 2055 scanner operated at 0.255 Tesla (10.86 $MH_z$) with a MR 3 software was used in conjunction with laboratory built solenoidal coils of diameter close to that of the plug, with windings of both ends extending the ends of the plug gave better homogeniety due to better filling factor and $\bar{B}_1$ fulx distribution in the region of the plug. Spin echo (SE) sequence was used with TR=1000ms, TE=40ms (few other TE's). 2DFT imaging technique was used. In order to enhance the image separation between oil and water, the aqueous portion was doped with $MnCl_2$ whcih significantly shortens $T_2$. The core material did not contribute to the image.

The figure (Cf. next page) shows the intrusion of $MnCl_2$ doped water, apparent as the black area, from the bottom displacing oil, the light area, out the top of the core plug for several increasing amounts of water. The results indicate that even for this water-wet core plug, the oil is heterogeniously displaced leaving quantities of oil behind which are larger than individual pores.

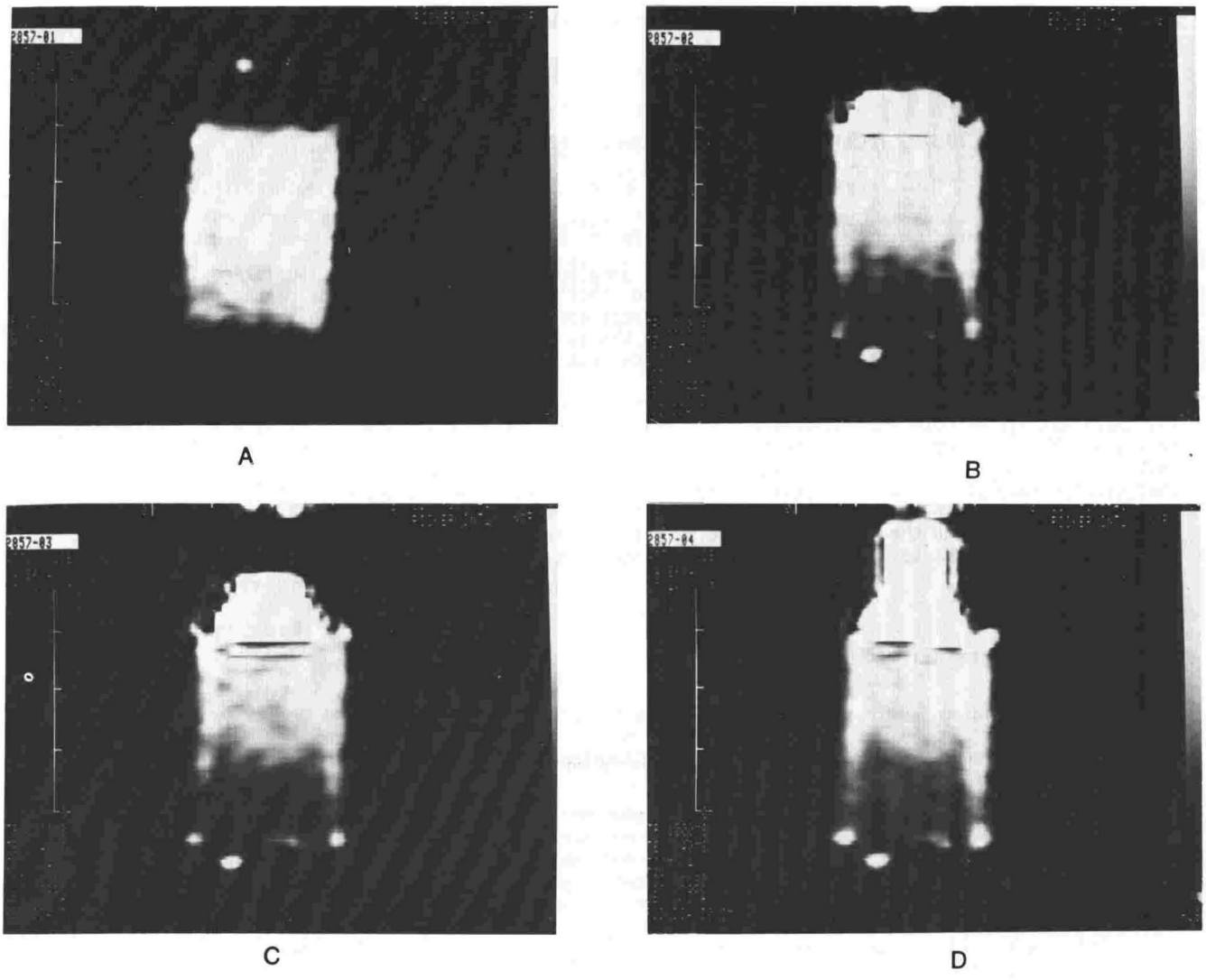


Fig. 3 Water displacing oil from the bottom of a water wet core. Water saturation: A ~ 0% PV. B ~ 17% PV. C ~ 38% PV. D ~ 50% PV

RAPID 13 POINT TECHNIQUE FOR ACCURATE T1 MEASUREMENT USING A WHOLE BODY NMR IMAGER

June T. Ruszkowski, Robert Lufkin, M.D., and William Hanafee, M.D.

Downstate Medical Center Program in Biophysics (JR)
UCLA School of Medicine (JR, RL, WH)

A unique determination of the spin-lattice relaxation time, T1, has been developed using a whole body NMR imager. A semilograrthmic plot of a 13 point data acquisition (In (Intensity) versus TR) results in a slope equal to $-(T1)^{-1}$. Simultaneous T1 measurements of up to 10 image points may be obtained in 3 minutes. The T1 measurements were standardized with chemical samples having T1 values in the physiological range. A uniform phantom was studied to confirm that the T1 measurements were constant throughout the imaging volume and reproducible over time. Early experience with normal volunteers and patients with known pathology indicate that the results are reproducible in a clinical setting.

The 13 point technique is a rapid, accurate, and reproducible method of T1 determination using an NMR whole body imager.

## MAGNETIC RESONANCE IMAGING TECHNIQUES FOR EVALUATION OF THE LUMBAR SPINE

Kenneth R. Maravilla, M.D., Crys Sory, M.D., Phillip Lesh, M.D., and Jeffrey C. Weinreb, M.D.

University of Texas Health Science Center at Dallas, Dallas, Texas

Several reports have shown that magnetic resonance imaging (MRI) is capable of visualizing lumbar intervertebral disc herniations in most cases. In these reports the sagittal view has proven to be the most efficacious while the transaxial view has shown severe limitations in visualizing the critical detail of the lumbar spine. The major limitations of MRI in the spine include poor signal-to-noise ratio, motion artifacts secondary to respiration, relatively thick sections resulting in partial volume degradation, and limited detail on the axial images.

Recently we have incorporated several improvements in our imaging techniques which have vastly improved the image quality of both the sagittal and, most importantly, the axial images. Using a 0.35 Tesla superconducting MRI unit, we have incorporated the use of a surface coil for routine imaging of the lumbar spine combined with 5mm thick contiguous thin sections and software with improved signal-to-noise ratio. These changes have resulted in vastly improved image quality and have also improved our ability to see critical detail of the lumbar spine including the nerve roots, dorsal root ganglia within the neuroforamina, the lumbar facet joints and the posterior lamina. These improved images may result in increased diagnostic accuracy and enable MRI to be competitive with CT scanning for evaluation of degenerative disease of the lumbar spine.

## MAGNETIC RESONANCE IMAGING (MRI) OF THE SPINE AND SPINAL CORD

Driss Cammoun, M.D., Charles Seibert, M.D., Christopher Morgan, M.D.[+], Stanley Smazal, M.D., Robert Edgar, M.D.[*], and Lewis Schiffer, M.D.

AMC Cancer Research Center, Craig Hospital[*], Radiology Imaging Associates, and University of Colorado Health Sciences Center, Denver, Colorado

The purpose of this study was to evaluate MRI imaging of the spine and spinal cord and to compare its diagnostic efficacy and clincal utility with conventional modalities. 181 consecutive patients with spine or spinal cord problems examined by MRI were included in this study. MRI images were obtained with 0.15T Technicare unit. In most cases, correlative studies (CT scan, Ultrasound, Isotope scans) were available for review. A variety of pulse sequences were used to display anatomical details and to enhance T1 and T2 contrast. Spinal cord and anatomical details were best evaluated by a short spin-echo technique (TE 30 ms and TR 500 ms) with 0.7 or 1.0 cm slice thickness. Pairs of sagittal images were required with 3 or 5 mm offsets between scans. Metastatic disease to vertebrae was differentiated from osteoporotic collapse by comparison between 30/500 and 45-90/1800 spin-echo pulse sequences. Metastatic lesions, demyelinization, cord tumors had a prolonged T2, one dural mass had isointense signal on the T2 weighted images. Hemorrhage was identified by increased signal on both 30/500 and 45-90/1800 spin-echo technique. Patients were examined in either head or body coils depending upon lesion location.

- -51 patients were studied for progressive post-traumatic cystic myelopathy (PPCM): 18 MRI positive and 33 negative with 9 false negative MRI on CT myelogram and 6 FN CT myelogram.
- -42 patients were studied for vertebral tumor: 24 positive; 1 FP; in 18 negative MRI showed 4 fractures. MRI was found more specific for metastases than bone scan.
- -30 patients were studied for Arnold-Chiari, craniocervical abnormalities or syrinx: 13 MRI positive; 17 negative.
- -27 patients were studied for spinal cord tumor or dural tumor: 6 MRI positive; 18 negative, 3 patients have other positve findings.
- -12 patients were studied and found positive for degenerative vertebral disease.
- -7 patients were studied for demyelinization: 3 MRI positive and 4 negative.
- -6 patients were studied for hematomyelia or AVM malformation: 2 MRI positive and 4 negative.
- -5 patients were studied for tethered cord: 3 MRI positive and 2 negative.
- -1 patient studied for osteomyelitis showed fracture with degenerative changes - no infection.

Technical factors that improved accuracy were: thin slices; axial as well as sagittal views; head rather than body coil; modified surface coil as opposed to conventional solenoidal coil; increased number of averages to improve S/N ratio; increasing phase encoding steps to 192 from 128; and use of head gradient in body coil to improve the spatial resolution. In summary, MRI was found to be efficacious for spine and spinal cord studies and provided new and correlative informations when compared with conventional imaging modalities.

Supported by a gift to the AMC Cancer Research Center from Steven L. Wenner.

## MAGNETIC RESONANCE IMAGING OF THE HEAD AND SPINE IN PATIENTS WITH NEUROFIBROMATOSIS

John W. Ross-Duggan, M.D., Kenneth R. Maravilla, M.D., Crys Sory, M.D., and Richard Suss, M.D.

University of Texas Health Science Center at Dallas, Dallas, Texas

We present a study utilizing magnetic resonance imaging (MRI) of the head and spine in patients with a known diagnosis of neurofibromatosis. In the majority of cases, correlative CT examinations were available for comparison.

MRI of the head showed good definition of multiple different types of lesions characteristically seen in neurofibromatosis. These included: optic glioma, bilateral acoustic neuroma, meningioma, infiltrating glioma, bilateral trigeminal nerve neuromas, and presumed cases of multiple hamartomas. In some cases, magnetic resonance showed abnormalities not visualized on CT and often, more than one type of abnormality was found in the same patient.

Imaging of the spine revealed good definition of intradural, extradural, and dumbbell neurofibromas. Intramedullary lesions such as ependymoma, glioma, and a case of hemangioblastoma were also well shown. Spinal magnetic resonance imaging proved far superior to non-contrast CT of the spine.

Although magnetic resonance imaging at this point shows limited specificity regarding tissue characterization, nonetheless it often showed different imaging characteristics among the various pathologic entities associated with neurofibromatosis. This spectrum of imaging characteristics sometimes enabled us to make a preoperative diagnosis with reasonable certainty. Magnetic resonance imaging has the added advantage of permitting evaluation of the entire CNS in a non-invasive and efficient manner. Specific imaging protocols used for evaluation of neurofibromatosis patients together with our correlative experience will be discussed.

## MRI IN THE DIAGNOSIS OF MULTIPLE SCLEROSIS

J. Martin Stewart, M.D.
O. Wayne Houser, M.D.
H. L. Baker, Jr., M.D.
Moses Rodriguez, M.D.
Peter O'Brien, Ph.D.

Mayo Clinic Radiology Resident
Clinic Staff Radiologist
Clinic Staff Radiologist
Clinic Staff Neurologist
Clinic Statistician

Over 130 cases of suspected multiple sclerosis (M.S.), myelitis, and optic neuritis were examined on a Picker .15 Telsa MRI scanner at the Mayo Clinic between November, 1983 and April, 1984. Using the diagnostic criteria of multiple sclerosis for research protocols (Annals Neurology, March, 1983), patients were categorized as having either definite or probable M.S. In addition, the extent of neurologic impairment of each patient was established using the Kyrtzke Expanded Disability Status Scale for M.S. (Neurology, November, 1983). These results were statistically correlated with MRI brain and cord lesion patterns. Factors such as CSF findings, number of attacks, evoked responses, and time of most recent attack were also correlated. Preliminary results show that of the patients referred for the above indications about half were eventually given the clinical diagnosis of M.S. About two-thirds of these had positive MRI scans. During the above time period, four cases of white matter disease consistent with M.S. were incidentally discovered by MRI as patients were being scanned for other indications including trauma and neoplasm. A small percentage of patients with definite M.S. displayed an unusual linear periventricular enhancement pattern. MRI provided paraclinical information useful to M.S. diagnosis in about two-thirds of cases and was critical to diagnosis in over one-fourth.

## LESIONS MIMICKING MULTIPLE SCLEROSIS ON MRI STUDIES

Murray A. Solomon, M.D., Phillip Sheldon, M.T., Lee Prevost, R.T., Kristi Stubbs, R.T.

San Jose MRI Center, San Jose, CA 95128

Magnetic Resonance Imaging has proven to be an efficient reliable technique for studying patients with multiple sclerosis. Despite the high sensitivity of MRI problems with specificity however, remain.

Review of Magnetic Resonance Imaging Studies performed at the San Jose MRI Center has revealed that several disease entities can present with multiple foci of increased signal intensity on $T_2$ weighted images and thereby mimic lesions usually associated with

multiple sclerosis. These disease entities inclued PML, post infectious encephalitis, Binswanger's Disease, Vasculitis, and Metastatic Disease. In addition there may at times be technical artifacts mimicking lesions. Representative cases will be presented and discussed.

CORRELATION OF MULTIPLE SCLEROSIS (MS) STAGING AND MAGNETIC RESONANCE IMAGING (MRI); DETECTING MS IN EARLY STAGES.

K.K. Wheatley, W.S. Yamanashi, P.D. Lester, A. Chan
City of Faith Medical and Research Center
Tulsa, OK 74137-1270

and

R. Richter
St. John Medical Center
Tulsa, OK 74104

This work has been conducted in order to (i) to evaluate effectiveness of MRI in the diagnosis of MS in the earliest possible stages (Kurtze Stage 1 and 2), (ii) to correlate MS lesions observed by MRI with those detected in other modalities such as clinical examination, CT, evoked potentials (visual, somato-sensory and acoustic), microbiological and immunological tests. Sixty MS patients, most of whom had positive clinical indication were scanned with MRI, a Picker MR VISTA 2055 scanner with a 0.5T max. superconducting magnet operated at 0.27 and 0.255T (proton frequencies 11.2 and 10.86MHz respectively), a MR-3 softward designed for 2DFT multislicing. The slice thickness was 0.7 cm, image pixel matrix was 256 x 256, number of image averaged was 2. Transaxial slices covering periventricular region as well as coronal and sagittal slices including the midline were obtained. Patients were divided into (a) severe (Kurtze Stage 7 to 8), (b) intermediate (Kurtze Stage 4 to 6) and mild with remissions (Kurtze Stage 1 to 3), from the clinical observations. The use of MRI is recommended to aid in confirming or excluding MS, after other modalities were performed. Results suggests that with the present imaging unit: (i) spin echo (SE) sequence with TE=120ms and TR=1000ms and TE=120ms and TR= 2000ms were found most useful for the detection of MS. (2) if the location of the lesion is suspected from previous examination/testing, the longer TE sequence with better contrast i.e., TE=120ms and TR=2000ms should be used initially, and if necessary, followed by a shorter TE sequence which is used to exhibit more anatomical details (but not necessarily the lesion). (3) when compared to CT, MRI was shown to be superior in all cases in visualization of MS. The superiority consisted of (i) MRI detected lesions in Kurtze Stage 1 to 3 patients where CT scans were false negative. (ii) when CT indicated multiple lesions, MRI detected larger number of localized lesions, which CT failed to detect. This occured frequently in Kurtze Stage 4 to 6. (iii) in severe cases with accompanying symptoms of quadriplegia (Kurtze Stage 7 to 8), MRI showed more details of larger streak-like lesions as will as smaller localized lesions compared to CT. (4) locations of lesions detected by MRI appears to confirm or supplement the visual or somato-sensory evoked potential tests. Examples of MRI of severe, intermediate, and mild with remission MS lesion are given on the next page.

Runge, VM, et al, Magnetic Resonance Imaging of Multiple Sclerosis, Amer. Jour. Roentgenology 5:691-702, 1984.

Young IR, Randell CP, Kaplan PW, James A, Bydder GM, Steiner RE, Nuclear magnetic resonance (NMR) imaging in white matter lesions of the brain using spin echo sequence. Jour Comp. Asst. Tomgr. 7:290-4, 1983.

Hazelwood CF, Jackson J, and Yamanashi WS, Imaging and relaxation measurements in human brain in "NMR Imaging" (Y. Jaklovsky ed.), Addison Wesley, New York, 1984, in press.



(i) Mild with remission
Kurtze stage 2

(ii) Intermediate
Kurtze stage 5

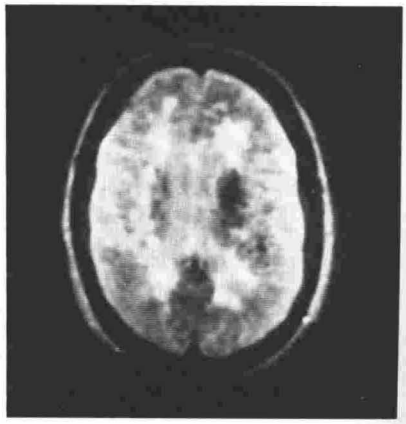

(iii) Severe
Kurtze stage 8

## MAGNETIC RESONANCE BRAIN IMAGING STUDIES IN SCHIZOPHRENIA

Henry A. Nasrallah, M.D., Nancy C. Andreasen, PH.D., M.D., Stephen C. Olson, M.D., Jeffrey A. Coffman, M.D., Val D. Dunn, M.D., James C. Ehrhardt, PH.D.

The University of Iowa, Depts. of Psychiatry and Radiology, and V.A. Medical Center, Iowa City, IA.

Several neuroanatomical abnormalities on computed tomography (CT) scans have been described in schizophrenia over the past few years. With the advent of Magnetic Resonance Imaging (MRI), it has become possible to examine additional brain regions in schizophrenia, using sagittal and coronal planes and enhanced tissue resolution to a degree not possible with CT scans. We used MRI to conduct a controlled study of cerebral size, corpus callosum dimensions and lateral ventricular size in schizophrenia.

28 schizophrenic males (diagnosed by DSM III criteria) mean age 32.3 years, and 21 volunteer males, mean age 27.7 years, consented to participate in the study. MRI was performed with a Picker .5 Tesla superconducting magnet. The midline sagittal (inversion recovery) view was used to measure 1) cerebral area 2) callosal area 3) lateral ventricular area 4) the callosum to cerebrum ratio 5) the ventricular to cerebrum ratio.

Significantly smaller ($p<.002$) cerebral area was found in the schizophrenic (93.6±9.4 $cm^2$) compared to the control group (102.8±9.8 $cm^2$), suggesting cortical atrophy or perhaps a different sagittal brain morphology in schizophrenia. In contrast to the CT findings of enlarged lateral cerebral ventricles in schizophrenia, no difference was found in this study of ventricular to cerebrum ratio in schizophrenic (3.9±1.5) and control (4.1±1.5) groups. No difference was also found in callosal area between the two groups.

The implications of the findings are discussed in light of previous CT and post-mortem findings. Comparisons of $T_1$ and $T_2$ in various cortical and subcortical structures are currently being conducted.

## DIFFERENCE OF T1 VALUES BETWEEN LEFT AND RIGHT HEMISPHERE IN SCHIZOPHRENIC DISORDERS

T.Fujimoto＊,Y.Yokoyama＊,A.Fujimoto＊,A.Okada＊,K.Yamamoto＊,A.Igata＊＊,T.Asakura＊＊,

＊Institute of neuroscience of Fujimoto Hospital,17−4,Hayasuzu Miyakonojo 885 Japan.＊＊University of Kagoshima.

Several CT studies in schizophrenic patients have shown morphologic asymmetries between hemispheres. We made a comparison between the T1 values of the left hemisphere and those of the right in schizophrenic disorders (DSM3,295) of patients in their thirties. We obtained 4 slices of T1 images from the coronal section perpendicular to the infraorbitomeatal line in 30 patients. Then the T1 values of all 10 areas were measured in each hemisphere. The size of the box of the T1 measurement is 5×5 pixels (3mm×3mm) and the slice thickness is 10mm. MR imaging system is Asahi Mark−J with a resistive magnet of 0.1T(4.5 MHz). The T1 values in the left hemispheres were plotted on horizontal axis (x axis) and the T1 values in the right hemispheres on vertical axis (y axis). Then we compared, on this two−dimensional plane, the group of points of schizophrenic patients with that of the normal controls of 5 males and 5 females in their thirties. We counted the number of points of patients outside the area enclosed by the points of normal controls. We used the Wilcoxon signed rank test to determine the differences between the T1 values of the left and right hemispheres. We reached the following conclusions which are charted on the table below.

| | area of measurment | number of points outside controls | Wilcoxon signed rank test | |
|---|---|---|---|---|
| | | | patient | control |
| 1 | frontal white matter | 10 (33%) | | |
| 2 | frontal white matter | 11 (37%) | $p<0.05$ | |
| 3 | head of caudate nucleus | 15 (50%) | | |
| 4 | parietal white matter | 10 (33%) | $p<0.05$ | |
| 5 | putamen | 24 (80%) | | |
| 6 | globus pallidus | 20 (67%) | | |
| 7 | temporal white matter | 16 (53%) | $p<0.03$ | |
| 8 | parietal white matter | 17 (57%) | $p<0.03$ | |
| 9 | medial thalamic nuclei | 13 (43%) | $p<0.001$ | |
| 10 | temporal white matter | 14 (47%) | | |

(1)Coronal section through rostal wall of lateral ventricle.
(2)(3)Coronal section through anterior limb of putamen.
(4)(5)(6)(7)Coronal section through putamen and globus pallidus.
(8)(9)(10)Coronal section through middle of thalamus.

## A REVIEW OF PATHOLOGICAL TISSUE $^1$H NMR RELAXATION TIMES FROM 1-100 MHz

**Paul A. Bottomley, Christopher J. Hardy, Raymond E. Argersinger, and Gwendolyn R. Allen**

**General Electric Corporate Research and Development Center,
PO Box 8, Schenectady, New York 12301**

**The normal tissue spin-lattice ($T_1$) and spin-spin ($T_2$) relaxation times from 1-100 MHz were recently reviewed as a function of NMR frequency, tissue, temperature, species, excision, and age(1). The study is now extended to published pathological tissue relaxation times in this frequency range, and comparison made with the normal $T_1$ dispersions to determine the significance of any differences. Data are tabulated according to species of origin along with claimed error, temperature, number of samples, description and source. To simplify analysis, pathologies are initially classified into six categories: tumours, implanted tumours, normal tissue from a tumour bearing organ (TBAL), normal tissue from a normal organ of a tumour bearing animal (TBAR), edematous tissue, and other miscellaneous disorders. Sufficient data is available to plot $T_1$ dispersions for muscle, liver, kidney, spleen, lung, intestines, breast, and brain tissues. Large scatter in the tumour and miscellaneous data (27%-37% and ~70% standard deviations, respectively) reflect the diversity and heterogeneity of tumours and other disorders whereas the TBAR and TBAL standard deviations were less than or equal to that of normal tissue. Results suggest that tumour tissue $T_1$ dispersions are significantly elevated in muscle, liver, and kidney relative to those of normal tissues, but less so in brain, lung, and breast (when compared with the normal fibrous value). Elevated $T_1$'s were also observed in miscellaneous disorders and edema with data often overlapping that from tumours. There does not appear to be any substantial difference between TBAL or TBAR data and the normal tissue dispersions, nor any significant species dependence of muscle or breast tumour $T_1$'s.**

1. **P. A. Bottomley, T. H. Foster, R. E. Argersinger, L. M. Pfeifer. Med. Phys. 11, 425-448 (1984).**

## THE CONTRIBUTION OF LIVER FERRITIN TO $T_1$ AND $T_2$ RELAXATION IN IRON STORAGE DISEASES.

Keith R. Burnett, Gerald L. Wolf, Edward J. Goldstein, Peter M. Joseph

The Dept. of Radiology,Hospital of the University of Pennsylvania and VAMC Philadelphia

Ferritin, a paramagnetic substance, constitutes the bulk of liver iron in patients with iron overload diseases and may be responsible for the extremely short relaxation times of the liver in such patients. To test this hypothesis, we measure proton $T_1$ and $T_2$ at 37 centigrade and 10MHz on serial dilutions (12.5-200mM) of Ferritin and Ferric Ammonium Citrate (FAC) in water and also in plasma. Also Ferritin (25-200mM) was uniformly suspended in tubes containing a 15% gelatin matrix. $T_1$ and $T_2$ was determined in vitro (10MHz) and the tube sets (Ferritin,FAC) were imaged at both .12T and 1.5T using a $T_2$ weighted spin echo technique (TR-1000ms, TE-40ms). The test solutions covered the range of total non-heme iron expected in patients with iron storage disease (22.9-117mmoles/L of liver) and the images were used to establish the relation between signal intensity and iron concentration. Abbreviated results are as follows:

| | | Plasma | | Gelatin | |
|---|---|---|---|---|---|
| | mM | $T_1$ | $T_2$ | $T_1$ | $T_2$ |
| | 12.5 | 774 | 402 | 714 | 333 |
| Ferritin | 50 | 359 | 241 | 416 | 178 |
| | 200 | 155 | 78 | 152 | 45 |

| | | Plasma | |
|---|---|---|---|
| | mM | $T_1$ | $T_2$ |
| | 12.5 | 141 | 90 |
| FAC | 25 | 75 | 52 |
| | 50 | 42 | 36 |

Images of Ferritin at each field strength showed enhancement at concentrations between 50-150mM (due to $T_1$ shortening)and some signal attenuation at 200mM (predominantly due to $T_2$ shortening). For all concentrations of Ferritin comparable to clinical levels, there was more signal intensity than appropriate for the postulated causal relationship. Therefore, Ferritin, which mole for mole is less effective in causing relaxation enhancement than FAC, may cause only a modest portion of the $T_1$ and $T_2$ shortening in iron overloaded liver. Other less abundant iron moeities in liver may have greater relaxation efficacy and could account for a large share of the observed effects of iron overoad in magnetic resonance proton images.

## MUSCLE RELAXATION TIME WITH DISUSE ATROPHY

LeBlanc, A., Evans, H. Marsh, C., Schonfeld, E., Ford, J., Schneider, V., Jhingran, S., Johnson P.

Baylor College of Medicine and NASA Johnson Space Center, Houston, Texas

Muscle atrophy is an attendant result of muscle diseases. The purpose of this work was to determine if changes in muscle relaxation times occur with nonpathological muscle atrophy produced by reduced limb load-

ing. The gastrocnemius muscles of rats, rear limb suspended for 30-90 days, were removed after sacrifice, and $T_1$ and $T_2$ determined using a Bruker CXP200 (200 MHz) superconductive magnet and a Radx Table Top T meter (20 MHz). In addition to relaxation times, % muscle $H_2O$ and muscle blood distribution were determined. In order to document blood distribution changes, labeled microspheres were injected into the left ventricle and following sacrifice, microsphere activity per gram of muscle was determined. Muscles from suspended rats were compared to nonsuspended control rats. There was no significant change in $T_1$ or $T_2$ at either frequency tested despite significant atrophy (-25%) and blood flow distribution (55% decrease in % cardiac output/g tissue) for the suspended rats.

The lower limbs of 6 normal volunteers were imaged pre and post 5 weeks of bedrest using a 6 MHz Bruker resistive magnet with head probe. The technique used was back projection using 120 projections per slice. Each projection consisted of a slice select pulse, a 90° read pulse and a series of 16, 180° pulses at 9 msec intervals. A total of 16 spin echoes were collected for each projection in 4 packets of 4 echoes each. An image was generated from each of the 4 packets and from these images a T2 and "spin density" image were calculated. The repetition time (1 sec) was not long compared to T1 so the "spin density" image retained some T1 dependence in addition to its primary spin density character. A series of 5 slices separated by 2 cm through the lower calf were obtained twice before and after bedrest. Slice thickness, pixel dimension and slice position were determined by simultaneously imaging a calibration jig. Five weeks of bedrest produced a mean 6% ($P = 0.05$) loss in crossectional muscle area while $T_2$, 48 msec, was not changed, similar to the rat results. These results suggest that nonpathological muscle atrophy will not significantly affect relaxation times of muscle.

## DO ELEVATED PROTON SPIN-LATTICE RELAXATION TIMES REFLECT LOSS OF STRUCTURAL ENTITIES IN MALIGNANCY?

S. S. Ranade

Biophysics Division, Cancer Research Institute, Tata Memorial Centre, Parel, Bombay: 400 012, India

Pulsed nuclear magnetic resonance (NMR) studies on human biopsy samples have shown that the proton spin-lattice relaxation times (T1 values) of surgically resected samples of human gastrointestinal tract cancers and uninvolved regions showed distinct differences, consistent with the basis of NMR characterization of the neoplastic state. Thus at 23.5 MHz for normal and malignant tissues the mean T1 values of 600 msec and 1000 msec respectively seen for a large number of gastrointestinal tract regions. In attempting to explore the basis of elevation of T1 values in malignancy, concomitant NMR studies and biochemical studies viz. protein and lipid estimation and gel electrophoresis were done. While the protein contents by themselves did not show any correlation with T1 values of normal and malignant state, the total lipids are seen to be lowered in many of the cancerous tissues of G.I. tract. Further agar gel electrophoresis showed that the lipo-protein as well as protein bands present in the normal and benign tissue samples were not in the tumor samples of epidermal carcinoma of oesophagus. This observation has been confirmed in tumours of gastrointestinal tract and appear to be promising in view of identification of biochemical factors like "vinculin" for maintenance of physical integrity of cell membrane. The observation supports the contention that increased T1 value in malignancy is due to loss of "structure" in malignant cells. Consequently, the increased "free" water content contributes to increase of T1 value.

## METHODOLOGICAL FACTORS INVOLVED IN MEASURING $T_1$s IN CULTURED CELLS.

S.A. McCormack and C.F. Hazlewood

Department of Physiology, Baylor College of Medicine, Houston, Texas 77030

The objective of our study was to identify the factors which might affect the measurement of water proton relaxation times ($T_1$s) in cultured cells. Using two human breast cancer cell lines, MDA-MD-231 and MDA-MD-435s, we examined five possible factors: (1) growth rates, (2) cell cycle distribution by flow cytometry, (3) the effect of trypsin-EDTA uptake, (4) viability and cell cycle distribution drift in the cell pellet with time after preparation, and (5) centrifugation forces and times required to remove the suspending medium without cell damage. With regard to factor (1), although 231 and 435s were easily recognized as "slow" and "fast" in routine maintenance in culture, detailed examination of growth rates over discrete 24-hour periods showed that this characteristic is too broad a parameter to correlate precisely with $T_1$s measured at one point in time primarily because it is a summation of processes occurring over days. On the other hand, factor (2) could be measured simultaneously with $T_1$ by using cells quick-frozen from the same cell suspension. By manipulating nutrition and density, the cell cycle distribution of the cells could be varied widely without resorting to drugs. In general, $T_1$s were higher in cell pellets with a high percent of cells in $G_0G_1$ than in those with higher percentages in S and $G_2M$. Factor (3) was without effect on cell cycle distribution or $T_1$s but did result in lower $H_2O$ content in pellets of 231 only at low

centrifugation rates. Factor (4) was tested at intervals up to 8.5 hours after pellet preparation. Cell cycle drift did not exceed 4% up to two hours after preparation. Viability over the entire period ranged from 81-97%. With regard to factor (5), in maintenance populations of 231, 11,800 g for 15 minutes removed the maximum amount of suspending medium without cell damage; for populations containing a high percent of cells in S, 5230 g x 10 minutes sufficed. 435s required 11,800 g x 20 minutes for maximum removal of suspending medium. We conclude that cell cycle distribution and the amount of suspending medium left in the cell pellets are the two main factors which must be controlled when cultured cells are investigated by NMR spectroscopy.

This work was supported by NCI Grant #CA36190, Robert A. Welch Foundation Q-390 and Cytocybernetics Laboratory Fund 360-G09850

## HYDROGELS AS ORAL NMR CONTRAST AGENTS AND PHANTOM MATERIALS

P.T. Beall, K.F. Mueller, C. Ebert, W. Good and J. Gore

Basic Pharmaceutics Research and Research Services, CIBA-GEIGY Corp., Ardsley, NY 10502;
Department of Diagnostic Radiology, Yale University Medical School, New Haven, CT 06510.

As much as 70% of radiological examinations deal with the gastrointestinal tract and it can be expected that a high percentage of human NMR imaging applications will as well. While numerous substances such as ferric chloride solutions, Geritol, vegetable oils, or solutions of gadolinium oxide have been used to visualize the lumen of the stomach and intestines, none have exactly the coating and filling properties which have made barium sulfate so useful in radiological applications. Criteria for the design of an oral imaging contrast agent should include (1) a high degree of contrast since the substance may be diluted in the GI tract, (2) the ability to coat and fill to visualize anatomical structures and abnormalities, and (3) most importantly, that it be inert and non-toxic in humans and not cause any adverse GI symptoms when ingested in large amounts. Considerable effort has been expended to design and manufacture a number of hydrophilic polymers for use as drug delivery systems in the pharmaceutical industry. These polymers based on 2-hydroxyethylmethacrylate or HEMA can be designed to produce very short $T_1$ and $T_2$ values for water entrapped in the polymer networks, they can be ground into beads and made into thick coating suspensions. We will report the $T_1$ and $T_2$ contrast potential of a number of these hydrogels in phantoms and present NMR images of the material in the GI tract of dogs at 6.4 MHz. Since the water content, crosslinking, and side group interactions can be synthetically altered, it may be possible to use several different hydrogels to construct organ phantoms as well. This work was supported by CIBA-GEIGY Corporation, Pharmaceuticals Division.

## THE CONTRAST TO NOISE RATIO: IMAGE QUALITY AND TISSUE DISCRIMINATION IN MRI AS A FUNCTION OF FIELD STRENGTH AND ADDED PARAMAGNETIC CONTRAST AGENTS.

Keith R. Burnett, Gerald L. Wolf, Paul Albert, Edward J.Goldstein

Dept. of Radiology, Hospital of the University of Pennsylvania and VAMC Philadelphia

The Contrast to Noise Ratio (CNR) is an important measure of image quality in magnetic resonance and describes the ease with which tissue pairs may be discriminated based on the field strength and $T_1$ or $T_2$ differences. For clinically important contiguous tissue pairs such as liver-fat, kidney-fat, or liver-kidney etc., the CNR increases with field strength up to at least 1.5T*. However, the addition of paramagnetic contrast agents (in vivo) could alter this relationship since many of these compounds demonstrate complex field related efficacy, especially in the 20-40MHz range. To study this problem, we injected (IV) $MnCl_2$, Mn-PDTA (chelate), Gd-DTPA (chelate), $Gd_2O_3$ colloidal particles, and saline (control) into rabbits and harvested selected "target" and non-target tissues. In vitro $T_1$ measurements were made on each sample in a unique variable frequency spectrometer at 12 different fields from 1-50MHz. For tissue pairs of interest, the $T_1$ data at each measured frequency was substituted into an equation yielding the expected CNR($T_1$) utilizing an imaging model (Partial Saturation 2DFT, acquisition times held constant)*. In addition, a "target" organ and its control counterpart was utilized as an artificial tissue pair simulating disease within that organ where the abnormal tissue differs little in $T_1$ relaxation from the host tissue and does not accumulate the contrast agent.

RESULTS: In almost all cases, the CNR($T_1$) increased severalfold as the field increased from .02T-1.2T(1-50MHz) regardless of the type of contrast agent employed or the tissue pair examined. The one major exception was kidney(Gd-DTPA)-fat where CNR($T_1$) became increasingly negative relative to its value at .02T. The CNR($T_1$) always increased with field when a contrast targeted organ was compared to its control counterpart. Thus, our data supports the contention that the in vivo behavior of potentially useful paramagnetic agents should not negatively impact on the positive aspects of imaging at higher field strengths. It appears that there is no field or field range where a particular contrast agent will be even more efficacious than the maximum limit of our test. The disease simulation data suggests that

abnormal tissue within an organ which is poorly discriminated from surrounding tissue on the basis of differences in $T_1$ relaxation should be more conspicuous after 1) the addition of a paramagnetic contrast agent and 2) as the field strength is increased from .02T to at least 1.2T.

*Hart HR, Bottomley PA et. al.: AJR 141:1195-1201 Dec. 1983

DETECTION OF CONTRAST ENHANCEMENT ON MAGNETIC RESONANCE IMAGING

Val M. Runge, M.D.; Ann C. Price, M.D.; Greg Thomas, B.A.; George Holburn, M.B.A.; C. Leon Partain, M.D.; A. Everette James, Jr., M.D.; Vanderbilt Department of Radiology.

Phantom and canine studies were performed to evaluate the effect of changes in pulse acquisition technique upon the detection of contrast enhancement.

A Technicare 0.5 tesla magnetic resonance imager with a 26 cm internal diameter RF coil was used for all studies. A phantom consisting of various concentrations (0.05 - 10 mmolar) of gadolinium (Gd) DTPA in saline was first imaged. TE was varied from 18 to 240 msec with TR ranging from 100 to 2000 msec using a spin echo type acquisition sequence. T1 and T2 calculations were also performed from imaging data. A canine model of blood-brain barrier (BBB) disruption was then employed to study the effect of changing pulse technique on detection of contrast enhancement in vivo. To create this lesion, an intravenous injection of 250ml of 20% mannitol (at 1cc/sec) was followed by an intra-arterial (internal carotid artery) injection of 125 ml of 25% mannitol (at 2cc/sec). This produces a transient disruption of the BBB as a consequence of the high osmolarity of the injected mannitol. This lesion is unaccompanied by significant cerebral edema, a fact confirmed by histological studies. Five minutes after the IA mannitol injection, 0.25mmol/kg Gd DTPA was injected intravenously. Pre and post-contrast scans with TE=36 and 72 msec and TR=250,500, and 1500 msec were compared, assessing the ability of each technique to detect contrast enhancement as well as the C/N and S/N ratios. Volume data acquisition techniques allowing the use of shorter TEs (such as TE=18msec) were also evaluated. In each animal, the area of disruption was confirmed pathologically with Evans blue stain following sacrifice.

In phantom studies, decreasing TE and TR improved detection of contrast, by increasing the difference in signal observed from very dilute solutions of contrast as compared with that achieving the greatest enhancement. This result is to be expected from equations relating signal intensity to the two parameters TE and TR (for spin echo acquisition techniques). From canine studies, short spin echo techniques also proved most efficacious for the detection of contrast enhancement, in particular the sequence with TE=36msec and TR=250msec. Shorter TE values allow further improvement in the signal difference between abnormal tissue containing Gd DTPA and surrounding normal brain. However these techniques impart additional problems in image interpretation. Further investigation with longer T2 weighted spin echo techniques (TE/TR = 90/1500) reveals that contrast enhancement can be observed using these sequences as well.

A wide spectrum of pulse techniques can be utilized to detect contrast enhancement on magnetic resonance imaging. The current investigation demonstrates both in vitro and in vivo the use of shorter TE and TR values to improve visualization of contrast enhancement, a circumstance which is expected from theoretical considerations. T2 weighted sequences may also show some signal enhancement with contrast administration, an observation with significant implications for clinical use of contrast agents. This is particularly true because of the current widespread use of T2 weighted techniques for routine clinical screening.

MAGNETIC RESONANCE IMAGING OF THE PROSTATE

Brian T. Larkin, M.D.
Thomas H. Berquist, M.D.
David C. Utz, M.D.

Department of Diagnostic Radiology
Mayo Clinic
Rochester, MN 55905

Goals of this study included; 1) defining the MRI characteristics of the normal prostate, prostate adenocarcinoma, and benign prostatic hypertrophy, 2) to evaluate optimal pulse sequences in imaging the prostate, 3) calculating $T_1$ and $T_2$ relaxation times for normal and pathological prostatic tissue, and 4) compare MRI results to clinical, pathological and CT results.

MRI of the pelvis was performed on 43 male patients with a 0.15 T resistive magnet using both IR and SE sequences. Twenty-six patients clinically suspected of having prostate ACA were scanned immediately prior to biopsy or surgery. Also studied were 10 patients with benign prostatic hypertrophy and 7 normal subjects. CT scans were obtained on 11 patients with ACA. Intracapsular neoplasm was well demonstrated on MRI with inhomogeneity and focal areas of prolonged $T_1$ and $T_2$ relaxation corresponding to pathologically proven areas of adenocarcinoma. Extracapsular extension, lymphadenopathy, and boney metastasis were accurately

demonstrated with MRI and in cases in which CT was available, MRI was clearly superior in defining the true extent of neoplasm. Benign prostatic hypertrophy was characterized by a relatively homogeneous signal texture and gland enlargement.

MRI is capable of demonstrating intra and extracapsular foci of pathology potentically allowing for more accurate diagnoses, staging, and subsequent selection of the appropriate treatment modality for prostate ACA.

## MR EVALUATION OF THE FEMALE PELVIS WITH A 0.5 TESLA SUPERCONDUCTING MAGNET

Anthony R. Lupetin, M.D., Nilima Dash, M.D., Rolf L. Schapiro, M.D., Ziad L. Deeb, M.D., Richard H. Daffner, M.D., Robert Sefczek, M.D.;

Allegheny General Hospital, Pittsburgh, Pennsylvania U.S.A.

In a nine-month period of time, seventy-five female patients have submitted to a magnetic resonance evaluation of the pelvic region. All studies were performed on the **Siemens' Magnetom,** a 0.5 Tesla superconducting magnet (liquid helium and nitrogen cooled) that has been operating at a nominal field strength of 0.352 Tesla. The radiofrequency system operates at 15 mHz.

Our usual pelvic MR technique consists of two sets of 1 cm axial sections weighted 1 each towards maximizing $T_1$ and $T_2$ contrast. The $T_1$ weighted set consists of a repetition time of 0.5 seconds with simultaneous echo acquisition at 35 and 70 msec. Five slices can be generated in 4.3 minutes. Our $T_2$-weighted consists of a repetition time of 2.1 seconds again with simultaneous echo acquisition at 35 and 70 msec. Seven slices can be obtained in 18.1 minutes.

The normal uterus on $T_1$-weighted images demonstrates a homogeneous midintensity signal. The cervix demonstrates a relatively hypointense appearance on $T_1$-weighted images. The vaginal walls demonstrate a midrange intensity while the mucous secretions within the vaginal canal are hyperintense on $T_1$ images. The normal ovaries demonstate a midrange intensity on $T_1$ sequences. Structures such as the fibrous round ligments and vascularity-laden broad ligaments are visible on $T_1$ and $T_2$-weighted sequences and change very little in appearance.

On $T_2$-weighted sequences, the endometrium demonstrates a hyperintense appearance while myometrium remains in midrange intensity. The endometrium and myometrium are separated by a low-intensity band that we believe represents the stratum basale layer of endometrium. The ovaries markedly increase in signal intensity on $T_2$-weighted images.

Uterine fibroids exhibit a hypointense appearance on $T_1$ or $T_2$ images due to the predominant fibrous and calcific nature of these masses. Gardner's duct cysts have been demonstrated within the lateral uterine walls and demonstrate a hypointense appearance on $T_1$ images. A case of rectouterine fistula has been observed with markedly low intensity air noted within the lower endocervical canal.

We believe MR will be useful in staging cervical neoplasms. We demonstrate MR criteria for urinary bladder and rectal invasion and demonstrate signal intensity changes that identify cervical carcinoma separate from normal cervical anatomy.

MR is demonstrated as an excellent modality in evaluating the wide range of benign and malignant ovarian pathology that occurs in the female pelvis. Ovarian carcinomas can be well visualized and internal septations and wall structures depicted. Their relationship to adjacent pelvic structures and information regarding invasion of local structures can be obtained. The presence or absence of ascites can also be determined.

Benign cystic teratoma of the ovary demonstrates a wide range of MR appearances with a characteristic appearance present when fluid, fat, and bony structures present within the tumor display three different signal intensities.

Endometriomas will present a homogeneously hyperintense appearance due to the large amount of blood within their centers.

We will also present the appearance of ovarian thecoma, fibroma, and hematoma.

MR is useful in depicting diffuse pelvic disorders and we will demonstrate its use in diagnosing pelvic inflammatory disease, pelvic hemorrhage, and widespread pelvic neoplasm. The increased signal intensity of the endometrium can be used as a signpost to demonstrate the position of the uterus when diffuse abnormatities are present.

## MAGNETIC RESONANCE TOMOGRAPHY (MR-T) IN NORMAL AND DIABETIC PREGNANCY

Francis W. Smith, Chester Kent and Hamish W. Sutherland

Departments of Nuclear Medicine, Aberdeen Royal Infirmary and Obstetrics and Gynaecology, University of Aberdeen, Scotland.

Using the Aberdeen 3.4 MHz MR imager, 87 pregnant volunteers have been examined, having a total of 98 examinations consisting of one sagittal and multiple axial sections made at 4 cm intervals. Three groups of patients have been examined following informed consent and approval of our local Ethical Committee. The first group comprised patients in the first trimester of pregnancy who subsequently underwent termination of pregnancy and in whom, in-utero fetal measurements (with MR-T), compared accurately with Ultrasound and actual measurement of the aborted fetuses. The other two groups comprised normal pregnancies and pregnancies of diabetic mothers who were imaged in the second and third trimesters on one or more occasion. This study was designed

to assess normal fetal development and the development of the fetus of the diabetic mother. Particular attention was paid to the assessment of fetal size, fetal liver, brain and lung and also to the measurement of fetal subcutaneous fat thickness from the buttock region.

Prior to 26 weeks of gestation, fetal movement and the relatively large amount of amniotic fluid contributed to poor detail in the images. After 68 weeks fetal movement was minimised by imaging the patients lying on their side rather than supine, a position that was adopted following the initial sagittal section.

MR-T images of the fetus provided accurate fetal measurements of diameter, area and circumference of head, chest and abdomen for dating fetal weight. When serial examinations were performed close correlation between serial uterine size and birth weight was found. The examination of the fetal brain showed that myelination of the basal ganglia could be identified as early as 34 weeks and serial measurements of fetal liver T1 showed a steady decline throughout gestation.

In diabetic patients the measurement of the fetal subcutaneous fat thickness correlated well with fetal birth weight. Fetal macrosomia and intra-uterine growth retardation were similarly easily identified.

## MAGNETIC RESONANCE IMAGING OF THE FETUS

Jeffrey C. Weinreb, M.D., Tom Lowe, M.D., Jesse M. Cohen, M.D., and Mark Cutler, M.D.

University of Texas Health Science Center at Dallas, Dallas, Texas

Because magnetic resonance imaging (MRI) involves no ionizing radiation and appears to be without significant risk, it would seem that it might be a useful imaging modality for the study of the fetus. The purpose of this study was to determine the ability of magnetic resonance to image fetal structures and to determine the most useful pulse sequences.

Twenty-five selected pregnant patients underwent MRI utilizing a .35 Tesla superconducting system. All patients were studied in the three orthogonal planes. Images obtained using a variety of spin echo pulse sequences were subjectively compared for their ability to depict fetal anatomy. Each fetus was examined to determine which of ten separate structures were visible in each case.

Little or no fetal anatomy was depicted in the first and second trimesters due to motion and diminuitive fetal parts. In the third trimester, the head, eyes, heart, liver, and limbs were almost always visible. Maternal sedation caused depression of fetal motion and resulted in improved imaging of fetal anatomy. T1 weighted images (i.e., those with a short TR and short TE) were best for imaging fetal anatomy in the third trimester because (a) the T1 differences between the fetus and the fluid and placenta are greater than the T2 differences, and (b) the selection of a shorter TR value results in shorter imaging time and less fetal motion during the time that data is acquired.

Preliminary experience suggests that because MRI is safe and can depict fetal anatomy, it may find a role as an adjunct to ultrasound in selected obstetrical cases.

## MAGNETIC RESONANCE IMAGING OF RENAL MASSES

Richard R. Remark, M.D.
Thomas H. Berquist, M.D.
Glen W. Hartman, M.D.
J. William Charboneau, M.D.

Department of Diagnostic Radiology, Mayo Clinic, Rochester, MN 55905

Twenty-six patients with a variety of renal masses were imaged with a .15 Tesla resistive magnet. This group included 11 renal cell carcinomas, 2 TCE's, a renal oncocytoma, 3 examples of metastasis, and 3 simple cysts. Single cases of angiomyolipoma, polycystic kidney disease, renal hematoma, acute focal bacterial nephritis, and a complicated cyst were also studied. Computed tomography and ultrasound were obtained in a majority of patients. Findings were correlated with pathological specimen and/or clinical and laboratory data.

The largest group consisted of 11 patients with renal cell carcinoma which magnetic resonance accurately staged in all cases. Tumor intensity varied with areas of low signal intensity corresponding to tumor necrosis. The majority of carcinomas consisted of high intensity signal comparable to that generated by renal cortex. Inversion recovery sequences provided better soft tissue contrast and corticomedullary differentiation than spin echo sequences. Calcification within a renal cell carcinoma appeared as an area of low intensity signal on spin echo images. The renal oncocytoma demonstrated prolonged $T_1$ and $T_2$ relaxation times, an appearance not seen in any of the carcinomas.

Recent hemorrhage was seen in 3 cases, including the patient with polycystic kidneys and acute focal bacterial nephritis and always appeared as a high intensity signal. Clotted blood in the periphery of a renal hematoma generated a high intensity signal while the serous portion exhibited a low intensity signal. Acute focal bacterial nephritis resulted in decreased relaxation times of the involved tissue with loss of the normal corticomedullary differentiation.

Magnetic resonance is a promising imaging technique for evaluating a variety of neoplastic, traumatic, and inflammatory renal processes.

## MR EVALUATION OF THE KIDNEY WITH A 0.5 TESLA SUPERCONDUCTING MAGNET

Anthony R. Lupetin, M.D., Nilima Dash, M.D., Rolf L. Schapiro, M.D., Ziad L. Deeb, M.D., Richard H. Daffner, M.D., Robert Sefczek, M.D.;

Allegheny General Hospital, Pittsburgh, Pennsylvania U.S.A.

In a nine-month period, fifty patients have submitted to magnetic resonance evaluation of their kidneys. All studies were performed on the **Siemens' Magnetom,** a 0.5 Tesla proton NMR imaging system utilizing a liquid helium and nitrogen-cooled superconducting magnet operating at a nominal field strength of 0.352 Tesla. The radiofrequency system operates at 15 mHz. Our renal MR protocol usually consists of two sets of 1 cm axial sections weighted one each towards maximizing $T_1$ and $T_2$ contrast. The $T_1$ set usually consists of a repetition time of .5 seconds with simultaneous echo acquisition of 35 and 70 msec. It takes 4.3 minutes to obtain five slices with this sequence. Our $T_2$-weighted sequence usually consists of a repetition time of 2.1 seconds with simultaneous echo acquisition of 35 and 70 msec. It takes approximately 18.1 seconds to obtain seven slices with this sequence. Coronal sections have been found particularly useful in evaluating the kidney and particular, the relation of renal lesions to the surrounding perinephric structures and adrenal glands.

The normal appearance of the kidneys on $T_1$ and $T_2$-weighted sequences will be discussed. On $T_1$-weighted sequences, striking cortical medullary differentiation is usually obtainable with hypointense renal medually tissue noted on a background of midrange intensity renal cortex. Renal vascular and collecting system structures tend to demonstrate a very hypointense appearance on $T_1$ images. On $T_2$-weighted images, this corticomedullary differentiation is usually lost with a generalized marked increased intensity of the entire renal parenchyma. In some cases, the kidneys approach the intensity of surrounding fat.

The renal capsule cannot be discerned, but the Geroda's fascia lines can be on $T_1$ and $T_2$-weighted sequences.

Magnetic resonance is a sensitive indicator of hydronephrosis without the use of paramagnetic contrast agents. We have not found MR to be a specific indicator of renal pathology but a sensitive technique in screening the kidneys for pathology. Renal cysts, and neoplams on occasion, will present similar intensity changes on $T_1$ and $T_2$-weighted images. In general, renal cysts are very hypointense on $T_1$ images and become hyperintense on $T_2$ images. Renal carcinomas tend to be slightly higher in intensity than cysts on $T_1$-weighted images and slightly less intense on $T_2$-weighted images, but this is not a constant rule with much overlap present. Renal lymphoma, metastatic deposit from carcinoma of the lung, and renal abscess all can produce a similar appearance to the entities described above. Renal infections are well demonstrated with MR, particularly xanthogranulomatous pyelonephritis and its extension into the adjacent psoas muscle and surrounding fat can be demonstrated with magnetic resonance.

We have found MR useful in detailing congenital anomalies of the kidneys and will demonstrate cases of horseshoe kidney, and crossed-fused renal ectopia. MR can demonstrate the appearance of the traumatized kidney with renal urinoma and hematoma visualized in several cases.

In general, we have not found MR useful in detailing abnormalities of the renal arteries, although in one case, fibrosmuscular hyperplasia was denoted with its typical beaded appearance. We have demonstrated left renal vein thrombosis in one case in which thrombus extended into the inferior vena cava.

## METHODS AND APPLICATIONS OF HIGH RESOLUTION MR IMAGING

**Thomas H. Foster, John F. Schenck, Howard R. Hart, Jr., and William A. Edelstein**

**General Electric Corporate Research and Development Center,
PO Box 8, Schenectady, New York 12301**

**The resolution of an MR image is determined by the magnitude of the applied imaging gradients. In this respect, resolution is independent of magnetic field strength and signal-to-noise ratio.**

**However, in practice it is precisely the available signal-to-noise ratio which limits the visualization of anatomic detail. As the imaging field of view is reduced through the application of stronger gradients, the higher inherent signal-to-noise ratio afforded by carefully designed surface receiver coils becomes essential if reasonable scan times are to be maintained.**

**Radiofrequency transmitter coils which produce uniform excitation throughout the region of interest are used in conjunction with smaller receiver coils. Solution of the technical problems associated with separate transmitter and receiver coils results in optimal performance.**

**High resolution techniques developed in our laboratory over the past 18 months have been integrated into clinical practice at several sites. Imaging slice thicknesses of 2.5-3.0 mm and pixel sizes of 0.4 mm x 0.4 mm have been successfully used. Imaging studies of various pathologies - including orbital tumors, spinal canal stenosis, degenerative and rheumatic joint disease, metastatic bone lesions, and TMJ abnormalities have been remarkably improved by these new high resolution techniques. Examples will be presented.**

## ALGORITHM AND CONTRAST CONFUSION WITH INVERSION RECOVERY MRI

Nolan Karstaedt, MB, BCh and Paul R. Moran, PhD

Borman Gray School of Medicine, Wake Forest University

The inversion recovery sequence has gained unwarranted disfavor in many instances of clinical practice. In large part this seems due to the unfortunate circumstance that images generated from the IR-sequence data are not true IR-images. The source of confusion is the physical interpretation and misidentification of two algorithmic defects. The first is a modulus-image reconstruction algorithm which is a "contract-obliterating" option, and the second confusion is in a phase-correction routine for reconstructing true IR-images as actual "in-phase" magnetization displays. This second option generates proper in-phase images, retains proper scale of contrast, but can invert the algebraic sign of image values under certain conditions. A series of actual scan examples demonstrate the effects and confusions observed in IR-sequences for MRI; they illustrate the considerable advantages to be gained, in practical clinical situations, if one generates true IR-images for IR-sequence data.

## CORRECTIONS FOR GEOMETRIC DISTORTIONS IN SPIN-ECHO IMAGES DUE TO FIELD INHOMOGENEITIES

John L. Patrick and E. Mark Haacke

Picker International, 5500 Avion Park Drive, Highland Heights, Ohio 44143

Static field inhomogeneities lead to geometrical distortion and pixel intensity non-uniformity in spin-echo images along the read gradient direction. Sekihara [1] has proposed a technique for the restoration of pristine image configuration from these problems. We have implemented his technique for 2DFT spin-echo sequences. We find that restoration from geometric distortions based upon the proper field maps can be largely achieved.

Sekihara's technique uses the information from a field plot to correct the image along the read gradient direction. It is assumed that the read gradient is sufficiently large so that there are no uniqueness problems. Even so, the field map itself will be geometrically distorted if extracted from images. We discuss the implementation of this technique for static field maps obtained from the following sources: direct magnetometer measurements, phase encodement of inhomogeneities from uniform density [2] phantoms and phase encodement of inhomogeneities from the object itself. We discuss these approaches and the correction to the maps themselves.

The reason for using the phase encoding technique on the object itself is the possibility of significant local susceptibility changes in the subject. This leads to inhomogeneities not accounted for in using a standard field plot. These "edge" effects are significant in phantoms and often non-negligible in in vivo studies of human subjects.

In conclusion, we find that it is possible in practice to extract an undistorted image from a field with significant static field inhomogeneities.

[1] K. Sekihara, M. Kuroda and H. Kohno, Phys. Med. Biol. 29, 15 (1984).
[2] P. Margosian and J. Abart, Proc. S.M.R.M., New York, N.Y. 495 (1984).

## NONSELECTIVE 180° PULSES WITH RESONANCE-OFFSET COMPENSATION

D. J. Lurie

Department of Bio-Medical Physics and Bio-Engineering,
University of Aberdeen, Foresterhill, Aberdeen, Scotland.

Most NMR imaging pulse sequences include nonselective 180° pulses. Conventional square 180° pulses may not be successful in an imaging experiment, where considerable resonance-offsets can exist due to main magnetic field inhomogeneity and to applied magnetic field gradients. Although composite pulses can be used to overcome this problem (1), they require specialised RF hardware and their use is not always desirable due to power absorption considerations (good composite pulses require 3-6 components).

In this work, resonance-offset compensation has been achieved by computer-aided optimisation of the 180° pulse shape. A geometrical model of the spin-system was used to calculate the effect of applying an arbitrarily-shaped radio-frequency (RF) pulse at increasing values of resonance-offset. The program changed the shape of the pulse in a systematic manner so that spin-inversion was achieved over as large a bandwidth as possible, the total length of the pulse being constrained. Good results were obtained by allowing the program to vary the relative widths and amplitudes of the subsidiary maxima and minima in a "variable-sinc" envelope (2).

The figure shows calculated inversion-efficiency as a function of normalised resonance-offset ($\Delta B/B_1^\circ$) and RF inhomogeneity ($B_1/B_1^\circ$), where $B_1$ is the peak RF magnetic field in the rotating frame, and $B_1^\circ$ is the value of $B_1$ corresponding to a 180° pulse. Dashed and solid curves are for square and shaped RF pulses respectively, the contours representing 99% (innermost), 97%, 95%, 90% and 80% inversion-efficiency. The use of a properly-shaped 180° pulse has extended the 99% contour by a factor of three in the resonance-offset direction. Although the shaped pulse is longer than the equivalent square pulse (with the same value of $B_1^\circ$), its duration is of the same order as a composite pulse but it is easier to implement and deposits less energy in the patient.

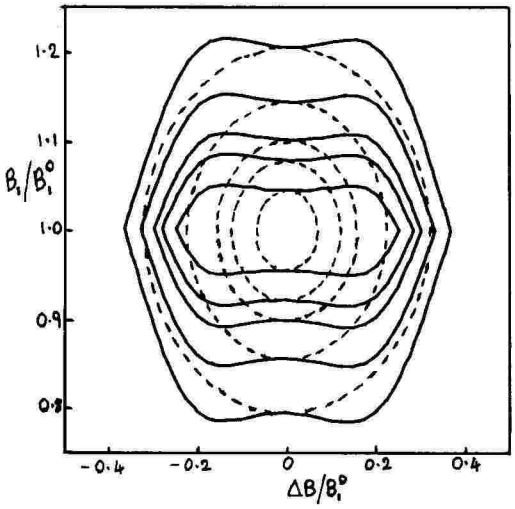


REFERENCES

(1) Shaka,A.J., Freeman,R. J.Magn.Reson. 55,487(1983)
(2) Lurie,D.J. Magn.Reson.Imaging, submitted.

## CLINICAL RESULTS OF THE HYBRID FAST SCAN NMR TECHNIQUE

R.E. Gangarosa, E.M. Haacke, M. Profeta, S. Albert, P. Coleman, P. Pattany, C. Huebner, D. Frizzell, J. Hahn

Picker International, 5500 Avion Park Drive, Highland Heights, Ohio 44143

E.M. Haacke[1,2] has proposed a fast NMR scan method which is a combination between echo planar and 2DFT techniques. He also demonstrated (3) that this variable frequency hybrid method allows a two or four fold reduction in scan time with comparable signal to noise (S/N) ratio in head imaging while maintaining resolution and contrast. The objectives of the present study are to test this method in a clinical setting and to provide preliminary evidence for its use in body imaging and with surface coils.

Initial clinical findings using this hybrid fast scan technique for head imaging of volunteers and patients will be presented. A Picker International Vista™ MR imager operating at 0.5T was used in our investigations. Our head imaging studies confirm the results of reference 3 in a clinical setting as follows:

1. Contrast and resolution are the same as 2DFT control images.
2. Imaging time decreases by two-fold or four-fold below conventional techniques.
3. There is an increase in white noise due to opening the bandwidth to allow for finer sampling in time. However, the overall noise, including systematic phase encoding problems such as motion, is distributed more uniformly throughout the image. Thus, with shorter scan times S/N may be better in regions affected by motion artifacts.
4. Somewhat greater chemical shift ghosting and geometrical distortion are observed especially in the presence of ferromagnetic objects. The latter effects are explained by the low read gradients used with the method in its early state of development, and could be seen also in control images with the same gradient amplitudes.

Preliminary results were also obtained with pulse sequences for body scanning. Images obtained in short intervals of about 1-4 minutes indicate greater spatial resolution than conventional images in the same scan time. Geometric distortion and chemical shift artifacts were reduced by using the low frequency hybrid technique. Motion artifacts which degrade conventional body imaging, were effectively reduced by dispersing them throughout the hybrid image.

Surface coils give rise to increased S/N ratio from a restricted volume of interest. The improved signal we obtained employing surface coils allowed hybrid imaging to be performed so that the normal loss in S/N associated with the technique was not important. However, the hybrid method is not as practical in cases with poor S/N ratio. The two-to-four fold decrease in acquisition time using hybrid imaging allows correspondingly larger TR values to be used in reasonable imaging times.

In conclusion, we find comparable image quality and contrast between hybrid fast scan and normal 2DFT images.

1. E.M. Haacke, SMRM, New York, August 1984.
2. E.M. Haacke, Application for U.S. Patient submitted.
3. E.M. Haacke et al, RSNA, Washington, D.C. Abstract #708, Radiology, November 1984.

## INTENSITY AND CONTRAST PROFILES IN MULTI-SLICE NMR IMAGING

S. David Smith, Ph.D.
Herbert C. Kranzer, Ph.D.
Russell K. Gusack, M.S.

Fonar Corporation, 110 Marcus Drive, Melville, New York 11747

In a multi-slice NMR spin-echo imaging sequence, tissue located at different depth within a slice is subjected to different levels of excitation and subsequent magnetization. In particular, the central region of each slice will give rise to a larger NMR signal than the wings of the slice, although in partial compensation the wing regions may contribute to two adjacent images rather than just one. Moreover, the effective repetition time $TR_{eff}$, which determines contrast in a typical $T_1$-dominated image, varies through the slice and from one slice to another. As a result, in certain circumstances a lesion which would be marginally visible if it occurred in the center of a slice may become invisible when it occurs between two slices, and in other circumstances the reverse may occur. The precise situation depends on a number of parameters, including number of slices, slice thickness, inter-slice spacing, order of excitation, RF wave shape and phase shift, as well as the usual echo time TE and actual repetition time TR. We have determined by computer simulation a set of optimal parameters for flattening the profiles of signal intensity and contrast as a function of depth. These optimal parameters are as follows:

1. Slice spacing approximately equal to slice thickness.
2. Order of excitation "by twos" including two externally adjacent dummy slices. For example, in a seven-slice sequence where slices numbered 1 through 7 are imaged, one excites these slices and also dummy slices 0 and 8 in the following "firing order": 1 3 5 7 0 2 4 6 8.
3. RF wave shape a three-lobed sinc function.
4. No RF phase shift between 90° and 180° pulses.

Intensity and contrast profiles are presented for this optimal case and for other cases obtained by varying one parameter at a time. In the optimal case, intensity variations through the slice are held to 5%, while the effective repetition time varies by less than 15%. Some other plausible parameter combinations used in NMR imaging are found to have intensity variations up to 60% and changes in $TR_{eff}$ of 100% or more.

## EARLY DETECTION OF INDUCED CANCER BY NUCLEAR MAGNETIC RESONANCE

N. Prasad,[1,2] J.E. Madewell,[1] J. Thornby,[2] R.N. Bryan,[1] S.C. Bushong,[1] and P. Ferro.[2]

Department of Radiology,[1] Baylor College of Medicine, Houston, Texas 77030, and Veterans Administration Medical Center,[2] Houston, Texas.

The objective of this study was to determine if parameters derived from Nuclear Magnetic Resonance (NMR) measurements could be used for early detection of malignancy. After inducing fibrosarcoma in mice using 3-methylcolanthrene (MC), NMR parameters were measured on tissues from mice sacrificed up to 14 weeks following insult.

Tumors were induced in 10-week old mice by a single subcutaneous injection of 0.1 ml corn oil containing 1 mg/ml MC into the right and left rear legs. A total of 24 mice were treated in this manner. Control mice and control legs on treated mice received similar treatment but did not receive MC. Mice were sacrificed on day 0 (controls), and on days 15, 30, 60, 75, 90 and 97 following injection. Muscle samples at the site of injection were removed and subjected to NMR testing using an IBM model PC-10 spectrometer.

The NMR parameters described in this report are T1 and T2 relaxation times and water content of the tissue samples. T1 values were measured by the inversion recovery technique ($180° - \tau - 90°$) at 10 MHz, and T2 values were obtained using the conventional Carr-Purcell-Meiboom-Gill pulse sequence. Water content was obtained by the gravimetric method.

For all three parameters there were no significant differences between control and treated legs through day 90. By day 97 tissues from the treated legs of all animals showed definite evidence of malignancy, and the three NMR parameters also indicated significant differences. Tissues from treated legs had higher values of T1 (565 vs. 454), higher values of T2 (75.0 vs. 44.8) and higher water content (77.3% vs. 71.6%).

The results of this study do not suggest that these three NMR parameters provide a means of detecting malignancy at an early stage. Not until the tumors were well-developed and evident morphologically were there any apparent differences between treated and untreated tissues in NMR parameters.

## THE INFLUENCE OF VARIOUS MACROMOLECULES ON THE PROTON RELAXATION RATES IN CSF

M.E. Castro,[1] D.P.J. Boisvert,[1] E.O. Treiber,[2] J.A. Lunt,[2] and P.S. Allen.[2]

Department of Surgery[1] and Applied Sciences in Medicine[2], University of Alberta, Edmonton, Alberta, Canada.

Imaging with nuclear magnetic resonance (NMR) is a sensitive indicator of the location and extent of brain

edema. Indeed, preliminary studies indicate that NMR imaging gives better definition of the extent and mass effects of edema than is achievable at present with x-ray computed tomography (CT). A major determinant in NMR images of the contrast of edematous brain tissue is the relaxation rate of protons in the edema fluid. In general, one expects the increased water content of edematous tissue to prolong both the longitudinal, $T_1$, and the transverse, $T_2$, relaxation times of the protons, in a relationship that is linear in water content. However, the presence of macromolecules, particularly proteins, in the edema fluid, as for example with vasogenic edema, will give rise to different water proton relaxation characteristics of that edema fluid.

Using pooled samples of cerebrospinal fluid as a model of edema fluid, we have evaluated the variation in proton relaxation rates ($1/T_1$ and $1/T_2$) as a function of the concentrations of albumin, gamma globulin (IgG) and human serum. The experiments were carried out at 100MHz and 37°C in a 30cm horizontal bore animal NMR imaging system and the individual protein concentrations, glucose concentration, electrolyte concentrations and pH were established in each sample.

The relaxation rates were found to vary linearly with protein concentration for each of the protein systems added, the rate of change of the transverse rate being approximately an order of magnitude greater than that for the longitudinal rate. Moreover, the rate of change was also increased as the size of the protein molecule increased. The parameters determined from a least squares fit to the experimental data are given below.

Table 1

| | $1/T_1$ linear regression | | | $1/T_2$ linear regression | | |
|---|---|---|---|---|---|---|
| | Intercept $s^{-1}$ | Slope $s^{-1}\ gm^{-1}\ \ell$ | Correlation coefficient | Intercept $s^{-1}$ | Slope $s^{-1}\ gm^{-1}\ \ell$ | Correlation coefficient |
| Albumin | 0.26 | 0.0015 | 0.994 | 0.39 | 0.018 | 0.993 |
| Gamma Globulin(IgG) | 0.27 | 0.0025 | 0.988 | 0.32 | 0.036 | 0.996 |
| Human Serum | 0.26 | 0.0037 | 0.991 | 0.43 | 0.050 | 0.997 |

## NMR STUDY OF HUMAN ERYTHROCYTE $T_1$ RELAXATION TIME

Abbey Strauss, M.D.*, Lawrence A. Minkoff, Ph.D.**, J.S. Rosenthal, M.D.*

* Beth Israel Medical Center, New York, N.Y. ** FONAR Corporation, Melville, N.Y.

Findings of $T_1$ values of normal human erythrocytes and those from patients with affective disorders are reported. These findings suggest an elevated $T_1$ value during periods of depression with a return to normal as depression remits under lithium therapy. This is consistent with previous observations made *in vivo* on the $T_1$ of brain tissue (1). Increased $T_1$ relaxation times have also been noted in normal women just before menses, with a marked drop after the onset of menstruation. This may be of some interest in the study of depression associated with Pre-Menstral Syndrome (PMS). Wide variations exist and may reflect a need to better refine laboratory techniques as well as the need to consider the extraordinary number of influences which can alter the erythrocytes physiochemical structure.

1 - R. Rangel-Guerra, H. Perez-Payan, L. Minkoff, and L. Todd: Nuclear Magnetic Resonance in Bipolar Affective Disorders. American Journal of Neuroradiology 4: 229 - 231, 1983.

## CONSTRUCTION OF ACCURATE T1 AND T2 PHANTOMS FOR MAGNETIC RESONANCE IMAGING

R. E. Hendrick and T. J. Provost

Department of Radiology, University of Colorado Health Sciences Center, Denver, CO 80262

Solutions of copper sulfate and agarose, in distilled water may be used to create tissue-equivalent T1 and T2 phantoms for magnetic resonance imaging. The concentration of copper sulfate is the primary determinant of T1 values, while the concentration of agarose determines the fractional reduction of T2 from the T2 value of the copper sulfate solutions. A matrix of $CuSO_4$-agarose solutions spanning the T1 and T2 values of normal tissues was constructed, and relaxation times were measured by multisequence techniques for each solution of 0.15 Tesla. Least squares fits to the matrix of T1 and T2 values as a function of $CuSO_4$ and agarose concentrations allow a simple method of constructing phantoms having any desired pair of T1 and T2 values for use of 0.15 Tesla. Effects of selective pulse profiles and field inhomogeneities on the measurement of T1 and T2 values are discussed.

FATTY INFILTRATION OF THE LIVER: *in vivo* QUANTITATION BY CONVENTIONAL AND CHEMICAL SHIFT MRI

M.S. Middleton, D. Stark, L. Grief, S. Saini, B. Rosen, and T.J. Brady

Massachusetts General Hospital and Harvard Medical School

Conventional spin echo (SE) and inversion recovery (IR) pulse sequences have proven insensitive for detecting fatty infiltration of the liver on the basis of image intensity or calculated tissue relaxation times. Recently, a number of proton chemical shift imaging sequences have demonstrated improved sensitivity for the detection of fatty liver. However, due to technical limitations, optimized conventional SE and IR sequences have not been evaluated, and no direct comparison of imaging techniques has been reported. Furthermore, quantitative applications of MR imaging have been extremely limited, and standardization of measurements has rarely been possible.

We compared the sensitivity of three conventional SE and IR sequences and two chemical shift sequences in rats to determine the accuracy for quantitating liver fat. An experimental model of fatty liver, analagous to human fatty liver, was created by feeding rats *1%* orotic acid for *1-3 months*. Forty-five rats with liver triglyceride levels ranging from *10 mg/gm* (normal) to *207 mg/gm* (severe fatty liver) were studied. Rats were sacrificed immediately after imaging, and liver specimens were analyzed for water and triglyceride content. Five MR imaging techniques were directly compared *in vivo*: conventional *SE 280/35*, *SE 2000/60*, and *IR 1500/400/15* sequences, a 3-D chemical shift *SE 250/50* sequence, and a Dixon 2-D phase contrast *SE 280/35* sequence. MR imaging was performed in a Technicare *1.47 Tesla* superconducting system with an *8 cm* bore. Animals were imaged alongside fat, water, and fat/water emulsion phantoms.

Machine error was studied by comparing signal intensity measurements of the three reference phantoms included on each image. MR measurements of liver signal intensity were correlated with biochemical determinations of liver fat content before and after normalization to the reference phantoms. Correlations between MR measurements and biochemical determinations were analyzed using the *t*-distribution for $df=n-2$ degrees of freedom.

The optimized IR sequence showed a good correlation with biochemically determined fat content ($r=0.83$, $P<0.0001$) and was superior to the optimized SE sequences. However, the Dixon method of 2-D spectroscopic imaging was the most sensitive and accurate technique ($r=0.93$, $P<0.0001$) for assessing fatty liver. The fat-water ambiguity inherant in the Dixon method may be partially resolved by simply referring to the in-phase data, which itself is crudely correlated with fat content.

**MR EVALUATION OF THE MEDIASTINUM WITH A 0.5 TESLA SUPERCONDUCTING MAGNET**

Anthony R. Lupetin, M.D., Nilima Dash, M.D., Rolf L. Schapiro, M.D., Ziad L. Deeb, M.D., Richard H. Daffner, M.D., Robert Sefczek, M.D.;

Allegheny General Hospital, Pittsburgh, Pennsylvania U.S.A.

In a nine-month period, 100 patients underwent magnetic resonance evaluation of their mediastinum for a wide range of pathologic entities. All studies were performed on the **Siemens' Magnetom,** a 0.5 Tesla superconducting proton NMR imaging system with a magnet field strength of 0.352 Tesla at the present time. The radiofreqency system operates at 15 mHz.

We have found $T_1$-weighted sections to be the most valuable in providing pertinent mediastinal anatomic information. Our ususal sequence consists of a repetition time of .7 seconds with simultaneous echo acquisition at 35 and 70 msec. Cardiac gating has been used on the last 50 patients and has been found to improve anatomic clarity. When $T_2$ sections are necessary, we utilize a sequence consisting of a repetition time of 2.1 seconds and simultaneous echo acquisition at 35 and 70 msec.

In all cases axial sections are obtained. Sagittal and coronal sections are found useful in evaluating the trachea, superior vena cava, and the bronchial structures.

We will demonstrate the usefulness of MR in diagnosing benign and malignant mediastinal disease. We have found MR a useful indicator of mediastinal pathology when bronchogenic carcinoma is present. It appears at least as sensitive as CT in detecting mediastinal lymph node enlargements and presently seems more accurate in detailing the affects of bronchogenic carcinoma on the mediastinal vascular structures, particularly the superior vena cava and innominate veins. MR has been found useful in staging esophageal malgnancies with sagittal or coronal images being able to detect the cephalocaudad extension of tumors. We demonstrate a case of primary tracheal carcinoma which was well demonstrated with magnetic resonance in the sagittal plane.

$T_1$-weighted sequences are particularly sensitive in detecting mediastinal lymphoma and we recommend the use of $T_1$ images to make this diagnosis as $T_2$ images lymphoma tissue will markedly increase in intensity and become isointense with mediastinal fat.

MR satisfactorily visualizes benign mediastinal disorders. We have experienced multiple cases of mediastinal thyroid extensions. These are particularly well-demonstrated with sagittal or coronal images. A neurofibroma of the right mediastinum and lung apex is demonstrated. Magnetic resonance was used to delineate

the extent of this neoplasm and to demonstrate lack of connection to the spinal canal without other invasive techniques having to be used.

We feel that MR may be the procedure of choice in screening the mediastinum for ectopic parathyroid adenomas. In the patient in which a neck adenoma has not been demonstrated with other imaging modalities, MR can sensitively detect these lesions by their midrange signal intensity as opposed to the flow void phenomena noted in mediastinal vascular structures and hyperintensity of mediastinal fat.

MR sensitivity in diagnosing vascular abnormalities will also be demonstrated with cases of superior vena caval thrombosis, innominate vein thrombosis and dissection, and dissection of the aorta, aortic coarctation, and aortic atherosclerotic aneurysm. A case of intracardiac sarcoma extending into the superior vena cava will also be demonstrated.

## MR IN PATIENTS REQUIRING MECHANICAL VENTILATION

Val D. Dunn, M.D., James M$^{c}$Gowan, M.S., R.R.T., John C. Godersky, M.D., and James C. Ehrhardt, Ph.D.

Departments of Radiology, Respiratory Therapy, and Surgery, University of Iowa Hospitals, Iowa City, Iowa

Over 20 individuals have been examined by MR while being mechanically ventilated with a fluidic ventilator at our institution. MR of patients on life-support systems has become almost routine with all of the necessary equipment being kept in the MR suite.

Before imaging patients who are ventilator-dependent, testing and modification of existing ventilator equipment and techniques was necessary. A Monoghan 225 SIMV Volume Ventilator (Monaghan Medical Corporation, Plattsburg, New York) was obtained and found mutually compatible with the .5 tesla Picker imaging system (Picker International, Cleveland, Ohio) without significant modifications. Only the stand and supporting equipment was changed to eliminate ferromagnetic materials. Because of the distance to the center of the magnet, an extended ventilatory circuit was needed to allow head imaging. This required the use of a Puritan-Bennett minimum dead space manifold and an increase in the ventilatory tidal volume in order to obtain proper $CO_2$ elimination. The usual tidal volume was increased 10-15% to compensate for an expanded volume of compressible gas in the lengthened tubing of the ventilatory circuit.

We have concluded that MR is not contraindicated in critically-ill patients. However, extra care, personnel, and equipment are required to monitor the patient and to ensure safety and proper ventilation. The main benefit of this study is to show that MR can safely be performed in a very important group of hospitalized patients; those requiring mechanical ventilation. MR in this population is not only important in evaluating disease and injury of the central nervous system, but also cardiovascular disorders. We have been able to demonstrate central herniation and brain injuries which would have been impossible without mechanical ventilation. It has also become apparent that in agitated patients there is a significant advantage in being able to pharmacologically paralyze patients to avoid motion degradation of images.

## VARIATIONS IN BREAST RELAXATION PARAMETERS WITH MENSTRUAL CYCLE

Thomas R. Nelson, PhD, Dolores H. Pretorius, MD, Lewis M. Schiffer, MD

Department of Radiology, University of Colorado, Denver and AMC Cancer Research Center, Lakewood, Colorado

Magnetic resonance imaging (MRI) of the breast offers potential quantitative measurement for both normal and pathological tissue. The purpose of this study was to determine whether relaxation parameters (T1 and T2) vary during a single menstrual cycle. It is well known that the composition of breast tissue changes during a woman's menstrual cycle, specifically water engorgement is greatest at 24-25 days since the first day of the last menstrual period (LMP). A young woman (GØ, PØ) on birth control pills was studied 8 times over one menstrual period. Transverse scans of both breasts were made on a Ø.15 Tesla MR imager. Estimations of T1 and T2 were calculated for breast tissues including fat and gland and as well as standards, using measurements based on pulse repetition times (.1Ø<TR<4.ØØ sec)(6 pts) and echo times (.Ø3<TE<.24 sec.)(8 pts). Breast glandular tissue showed a progressive rise in T1 from .45Ø±.1ØØ sec. to a peak of .68Ø±.Ø9Ø sec at day 25. There was no significant change in T2 (.Ø7Ø±.Ø11 sec) during the same period. Breast fat showed no significant variation in T1 (.2Ø5±.Ø35 sec) or T2 (.Ø86±.Ø12 sec) during the study. This preliminary work suggests that breast relaxation parameter measurements are affected by the time in the menstrual cycle at which measurements are made. Thus, accurate identification of pathology is potentially dependent on the time in the cycle that MRI is performed. Additional work needs to be done to more completely characterize the variations in normal breast tissues as a function of menstrual cycle, age and drug therapy.

This work was supported by a gift to AMC from Tony Cook

## MAGNETIC RESONANCE OF THE LIVER WITH A A 0.5 TESLA SUPERCONDUCTING MAGNET

Anthony R. Lupetin, M.D., Nilima Dash, M.D., Rolf L. Schapiro, M.D., Ziad L. Deeb, M.D., Richard H. Daffner, M.D., Robert Sefczek, M.D.;

Allegheny General Hospital, Pittsburgh, Pennsylvania U.S.A.

One hundred and fifty patients have undergone a magnetic resonance evaluation of their liver in a nine-month period. All studies were performed on the **Siemens' Magnetom,** a 0.5 Tesla superconducting liquid helium and nitrogen-cooled superconducting magnet operating at a nominal field strength of 0.352 Tesla. The radiofrequency system operates at 15 mHz.

Our hepatic MR protocol consists of two sets of axial 1 cm sections weighted one each towards maximizing $T_1$ and $T_2$ contrast. Our $T_1$ set usually consists of a repitition time of 0.5 seconds with simultaneous echo acquisition at 35 and 70 msec. Five slices can be obtained in 4.3 minutes. Our $T_2$-weighted set usually conists of a repetition time of 2.1 seconds with simultaneous echo acquisition again at 35 and 70 msec. Seven sections can be obtained in 18.1 minutes.

In general, we have found that coronal and sagittal images tending not to add additional diagnostic information except when intrahepatic processes extend outside of the liver and engage the region along the diaphragmatic surfaces. In these cases, coronal and sagittal images are particularly helpful.

We have found MR to be a sensitive but not specific screening technique for focal hepatic pathology. All focal lesions evaluated in our study demonstrated similar intensity changes on $T_1$ and $T_2$-weighted images with most lesions hypointense on $T_1$-weighted images and hyperintense on $T_2$-weighted images. This included metastatic disease from multiple primary lesions, hemangioma, biloma, lymphoma, and abscess.

Diffuse hepatocellular lesions such as hepatic cirrhosis or fatty liver were not well demonstrated with the usual spin echo sequences, although they could be demonstrated with the use of chemical shift spin echo sequences.

We have found magnetic resonance extremely sensitive to the presence of metal deposition within the liver and demonstrate a case of transfusion hemosiderosis where the paramagnetic affect of the large amount of iron present markedly depressed the hepatic MR signal.

We have not found MR particularly useful in evaluating the biliary tree whether normal in dimension or dilated. $T_2$-weighted sequences tended to better demonstrate dilated biliary structures, but this was not a constant rule.

We have found MR useful in evaluating intravascular abnormalities within the liver and demonstrated a case of left portal vein thrombosis and several cases of inferior vena caval thrombosis.

## MRI OF THE ILIOPSOAS MUSCLES

Jeffrey C. Weinreb, M.D., Jesse M. Cohen, M.D., and Kenneth R. Maravilla, M.D.

University of Texas Health Science Center at Dallas, Dallas, Texas

Using a .35 Tesla superconducting MRI system, fifteen normal subjects were imaged and the appearance of the iliopsoas muscles was defined. MRI and CT were also performed on sixteen patients with demonstrable iliopsoas disease. Seven patients had tumorous involvement of the muscles, six had an inflammatory disease, one had retroperitoneal hemorrhage, one had bilateral hypertrophy, and one had an indeterminate infiltrated condition. In these sixteen patients, MRI permitted better delineation of the muscles than CT in six, better depiction of pathology in six, and better definition of the extent of disease in six. Neither MRI nor CT provided the ability to identify a specific disease process in the absence of clinical data. Transverse MR images alone almost always provided the necessary data to determine the origin and extent of disease. T1 weighted images provided optimal contrast between muscles and adjacent normal tissues, while T2 weighted images were more useful for depicting disease within the muscles themselves. The results indicate that MRI of the iliopsoas muscles can provide much of the same information provided by CT and, in some cases, MRI may offer some advantages compared to CT.

## HIGH RESOLUTION MAGNETIC RESONANCE IMAGING OF THE FOOT AND ANKLE

Murray A. Solomon, M.D., Philip E. Sheldon, M.T., Kristi Stubbs, R.T., Lee Prevost, R.T.

San Jose MRI Center, San Jose, CA 95128

Utilizing a high resolution software package (8 average, 256 x 256 matrix) on a Diasonics MT/s 0.35 T superconducting imager, exquisite anatomic detail of normal and pathologic anatomy has been obtained in the foot and ankle. The spatial resolution with high resolution techniques approximates that of CT and the soft tissue contrast resolution is markedly improved. MRI has been useful in evaluating cases of bilateral achilles tendon xanthomas, post-traumatic scarring about the peroneal tendon sheats, post-traumatic scarring about the malleolar ligaments, plantar soft tissue masses, and osteochondrites dissecan of the dome of the talus. MRI has not proved reliable in studying Morton's neuromas. Representative cases will be presented and discussed.

MAGNETIC RESONANCE IMAGING (MRI) OF SMALL ANATOMIC REGIONS, JOINTS AND VASCULATURES AT 0.255T USING SMALL COILS OF VARIOUS SIZES AND GEOMETRIES.

W.S. Yamanashi, R.D. Hartman, A.M. Sy, C.R. Crandal and P.D. Lester
Department of Diagnostic Imaging and Radiation Medicine, City of Faith Medical and Research Center, Tulsa OK 74137-1270

MRI receiving coils of various geometry and size including, loops, cross configured quad loop and modified quad loops and solenoids were designed and constructed for improvement of image resolution in small anatomic regions over conventional head or torso coils. Larger diameter loop coils were developed for visualization of breast and large joints; smaller loops for opthalmic and thyroid imaging. Coils consisting of four loops, with transverse axes of two of the components crossed, were designed for joints and vasculatures in limbs and extremeties. Wrapped around saddle coils and solenoid coils were built for imaging of small animals (i.e. rats and mice). The central resonance frequency, impedance, and phase angle of the coils were measured with a Hewlett Packard H.P. - 4193A vector impedance analyzer. The advantages of using small coils for small volume of interests (VOI) are: (1) better signal to noise ratio (S/N) due primarily to the improved filling factor; (2) better resolution over VOI; and (3) more degrees of freedom in adjusting the coil to VOI. The quad loop coil was shown to be useful when a bent object must be imaged, or when a object must be inserted from two orthogonally seperated position. The small diameter solenoid coil was constructed to be used in small animal imaging or oil/water distribution study for an oil industry where RF homogeniety is maximally required over the sample volume. The small wrapped around saddle coil was used for imaging of extremeties (esp. joints and vasculature). Example of MRI of a human head obtained using a 12cm loop coil (Figure 1), of an orange using a cross configured loop coil (Figure 2), and of a hand using a wrapped around saddle coil (Figure 3) are illustrated on the next page. Resolution improvement over the head coil was visualized with the use of a standard resolution phantom (Picker 175-147). All images were taken with a Picker MR VISTA 2055 scanner with one of these coils in the place of the head coil, spin echo (Hahn) sequence with TR = 1000 ms, TE = 40 ms with 2DFT reconstruction was used. The transmitter was returned to each different coil before the scan.

Yamanashi et al continued

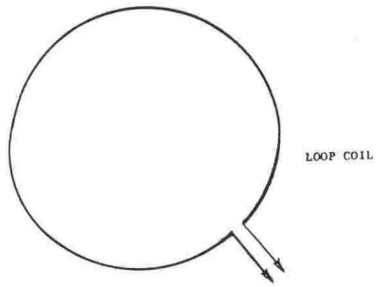


Figure 1
A sagittal image of a head obtained with a 7" diam. 2 turn loop coil placed on the anterior of the face on a formed pad insulator.

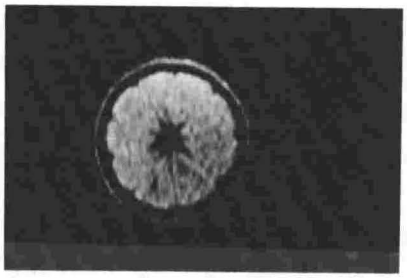

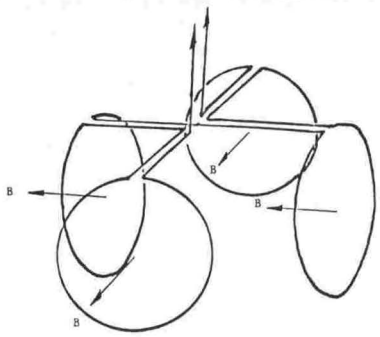


Figure 2
A transverse image of an orange obtained with a four loop, 4" diam. cross configuration coil. The sum of the $\bar{B}$ vectors was oriented orthogonal to $\bar{B}_o$.

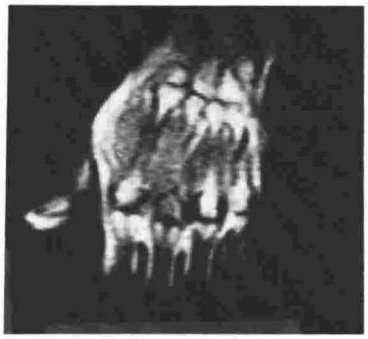

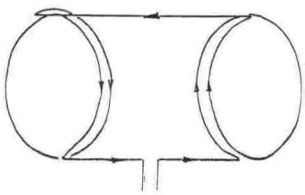


Figure 3
A image of a hand exhibiting some vasculatures and bones, taken with a wrapped saddle coil 4½" diam., 4" length.

All images taken with these coils in the place of the head coil (impedance matched) of a Picker MR VISTA 2055 scanner operated at 0.255T, 10.86 $MH_z$, with SE sequence, TE=40 ms, TR=1000 ms, 2DFT reconstruction, matrix=$256^2$, averaging=2.

REFERENCES
T.W. Redpath, Crossed Ellipse coils for NMR Imaging of the Head and Neck, Magnetic Resonance in Medicine 1, 232-4 (1984).
P. Mansfield and P.G. Morris, NMR Imaging in Biomedicine, Academic Press, London, 1982, pp. 280-296.
D.G. Gadian, Nuclear Magnetic Resonance and Its Application to Living Systems, Clarendon Press, Oxford, 1982, pp. 159-185.
L. Axel, Surface Coil Proton NMR Imaging, Magnetic Resonance in Medicine 1, 84-5 (1984)
W.S. Yamanashi, J.D. Forster, et al. Design Criteria for Low Frequency RF Phantoms Used in Clinical NMR and Tumor Hyperthermia, IEEE Ann. Rept. Conference on Electrical Inculation and Dielectric Phenomence, 83 CH 8902-6, (1983) pp. 356-362.

## MAGNETIC RESONANCE (MR) IMAGING IN TREATMENT PLANNING

Alexander C. Mamourian, M.D., John A. Stryker, M.D., David E. Cunningham, Ph.D., William A. Weidner, M.D.

The Milton S. Hershey Medical Center, The Pennsylvania State University, Hershey, PA 17033

Twenty five patients with known cancer were evaluated with MRI to determine the accuracy of radiation therapy treatment portals determined by conventional means. Propylene glycol filled tygon tubing was applied directly over the skin marks used for therapy. Patients were then positioned in the MR scanner as they were in treatments. Using a 0.15 T resistive scanner with TR 500 TE30 patients were scanned in axial, coronal, and sagittal planes in the region of interest. The tubing appears as a white dot permitting the spatial relationship of the portal to the tumor to be evaluated. Brain tumors as well as cancers in the chest, abdomen, and pelvis were included in the study. Preliminary results indicate that this will be most useful in the abdomen and pelvis where sagittal images provide additional information to CT images thus permitting more accurate localization.

## "F-19 AND H-1 DUAL NUCLIDE MRI FOR DELINEATION OF MYOCARDIAL INFARCTION"

Nunnally RL, Babcock EE, and Horner SD

Department of Radiology and Biomedical Magnetic Resonance Center, The University of Texas Health Science Center at Dallas, Dallas, Texas 75235

Water-soluble $^{19}F$-labeled compounds are promising MRI contrast agents for the evaluation of tissue perfusion because there is normally no background of $^{19}F$ in soft tissues. Using a salt of trifluoromethyl sulfonic acid, in a perfused rabbit heart model, $^{19}F$ MR images can be obtained for control, regionally infarcted, and reperfused protocols. Due to the low levels of fluorine which are present in the myocardium under the conditions used, the $^{19}F$ images have a low signal-to-noise ratio. Since the magnetogyric ratios of $^{19}F$ and $^{1}H$ are similar, it is simple to obtain good $^{1}H$ MR images utilizing a probe optimized for $^{19}F$ observation. Normalization of the signal intensities of the two image sets ($^{19}F$ and $^{1}H$) with subsequent subtraction of the $^{1}H$ image data from the $^{19}F$ image data yields a resultant image clearly delineating the perfusion defect present in a permanently ligated infarct model. Furthermore, in the reperfusion model, a perfusion defect persists when flow to the left coronary arteries is reestablished following 15 minutes of arterial occlusion. Images were obtained at 4.25 Tesla, which corresponds to a frequency of 167.5 MHz for $^{19}F$ and 178.1 MHz for $^{1}H$. This "dual nuclide subtraction imaging" technique is particularly advantageous for the combination of $^{19}F$ and $^{1}H$ because of the closeness of their respective resonance frequencies at any constant magnetic field. The distribution of the $^{19}F$ label is perfusion dependent and the resultant substracted image demonstrates that the infarcted region "border zone" is a sharp and narrow one. Even in the reperfusion studies, the persistent perfusion defect indicates a well-defined border zone. The use of such a technique for the early evaluation of myocardial infarction could have an impact on the clinical management of such cases.

## "THE CHARACTERIZATION OF A F-19 LABELED AGENT FOR THE EVALUATION OF TISSUE PERFUSION BY F-19 MRI."

Horner SD, Babcock EE, Storey CJ, and Nunnally RL

Department of Radiology and Biomedical Magnetic Resonance Center, The University of Texas Health Science Center at Dallas, Dallas, Texas 75235

A number of properties and parameters of the meglumine salt of trifluoromethyl sulfonic acid (TFSA) have been determined for characterization of this agent in applications to $^{19}F$ and dual nuclide subtraction of MRI in the evaluation of organ perfusion in situ and in vivo. For protocols using the $^{19}F$-labeled agent, the concentration of the TFSA in the perfusing solution is 190 mM. Tissue levels which result from this protocol have been determined by chemical analysis and by high resolution of $^{19}F$ NMR. Data from a set of solutions varying in TFSA concentration were obtained using identical NMR parameters. This data was then integrated and used as calibration data with which data from tissue samples were then compared. Table 1 gives the

results so determined. $^{19}F$ longitudinal relaxation rates have been determined for TFSA in solution and in myocardium. At the 4.25T field used, these values are 4.3 seconds and 4.1 seconds, respectively. It is of interest to note that these values differ little from one another, and this is probably a result of the fact that TFSA remains extracellular. TFSA has been shown to have a relatively low in vivo toxicity and initial results of $^{19}F$ imaging in a perfused rabbit heart model indicate that this agent has potential as a perfusion marker in MRI applications.

TABLE 1

Tissue Concentration of TFSA*

| Chemical Analysis | NMR Technique |
|---|---|
| 54 mM | 51 mM |

*Based on 80% of wet weight of tissue being water.

## IN-VIVO C-13 NMR OF GLUCOSE METABOLISM IN MONKEY BRAINS

Bruce E. Hammer[1], William Sacks[2], Michael J. Hennessy[1], Rodney E. Bigler[3], Shirley Sacks[2], Arthur Fleischer[2], and Pasquale B. Zanzonico[3]

1-Intermagnetics General Corporation, MRI Laboratory, Troy, NY
2-Nathan S. Kline Institute for Psychiatric Research, Orangeburg, NY
3-Cornell University Medical College, New York, NY

The objective of this study was to investigate cerebral glucose metabolism of the monkey brain by C-13 NMR. Metabolic pathways of C-13 labeled glucose can be deduced by analyzing the proton decoupled C-13 NMR spectrum. The relative concentrations of metabolic intermediates can, in principle, be determined by measuring the area under each peak in the NMR spectrum.

An Intermagnetics General Corporation (IGC) 3.0 Tesla, 25 cm warm bore superconducting magnet operating at 2.1 Tesla was used for these experiments. Proton and carbon-13 radiofrequency probes were operated at 90.303 and 22.707 MHz, respectively. Carbon-13 free induction decays (FID's) were 2 K points in length, sampled at 20-40 usec/point, and digitized in a 12 bit A/D converter. The FID's were zero filled, weighted with a gaussian filter, and Fourier transformed. Four grams of (C-13)-1-glucose was intravenously administered to a Rhesus monkey sedated with Ketamine hydrochloride. Proton decoupled C-13 spectra were averaged every 15 to 30 minutes over a ninety minute period.

Carbon-13 spectra were acquired during ninety minute experiments. Metabolism of (C-13)-1-glucose should ultimately label glutamate and glutamine of the brain. This is a consequence of glucose entering the tricarboxylic acid cycle where α-Ketoglutarate is metabolized into glutamate[1-3]. The glutamate-glutamine pool size is relatively large so that C-13 carbons which enter this pool are slow to re-enter the TCA cycle. Consequently glutamate-glutamine C-13 signals should be observed after glucose is metabolized. The spectra obtained are interpreted in view of this mechanism.

References:

1 Sacks, W. (1965). Cerebral metabolism of doubly labeled glucose in humans in vivo. J. Appl. Physiol. 20: 117-130.

2 Sacks, W., Sacks, S., Badalamenti, A., and Fleischer, A. (1982). A proposed method for the determination of cerebral regional intermediary glucose metabolism in humans in vivo using $^{11}C$-glucose and positron emission transverse tomography (PETT). I. An animal model with $^{14}C$-glucose and rat brain autor adiography. J. Neurosci. Res. 7: 57-69.

3 Sacks, W., Cowburn, D., Bigler, R.E., Sacks, S., and Fleischer, A. (1985). Evidence for the cerebral uptake in vivo from two pools of glucose and the role of glucose-6-phosphatase in removing excess substrate from brain. Neurochem. Res. 10: 117-144.

## CHEMICAL SHIFT IMAGING IN THE FACE OF FIELD INHOMOGENEITIES

John L. Patrick and E. Mark Haacke

Picker International, 5500 Avion Park Drive, Highland Heights, Ohio 44143

We present a technique for the separation of water and fat which can operate in the face of static field inhomogeneity and differing tissue susceptibility. This allows the separation to be achieved over large spatial areas where the static field inhomogeneity may be a significant fraction of the chemical shift. The technique also allows extraction of the static and susceptibility related field inhomogeneities.

Our results establish upper bounds on the subject's effect upon the static field homogeneity and provide a technique for exploring this problem. We present whole body water-fat separated images and

contrast these with attempted water-fat separation by techniques which do not account for field inhomogeneities. The elimination of static field problems by imaging uniform phantoms is also discussed. We find that the field inside the phantoms change by several ppm across the phantom edges due to changes in susceptibility. This edge effect on the static field was also confirmed by direct magnetometer measurements.

To avoid the above problems, we utilize similar methods which encode the field inhomogeneity and chemical shift in the phase. Three images are used to extract the three unknowns: water signal, fat signal and total static and susceptibility related field inhomogeneities. The resulting images, especially those at high field, are significantly improved by eliminating the field inhomogeneity effects.

Recently, several authors [1] have detailed techniques for the measurement of static field inhomogeneity utilizing a spin-echo 2DFT experiment in which the inverting 180° pulse is shifted by a small time interval "$\varepsilon$". The resulting phase image will have a position dependent static field contribution given by: $\phi = 2\gamma\Delta B$. This basic sequence has also been utilized by several authors [2] to achieve water-fat separation by setting $\phi = \pi$ for $\Delta B$ equal to the chemical shift difference between water and fat. The resulting scan then yields water minus fat and may be added to or subtracted from a normal spin-echo scan (water plus fat) to yield water or fat images. This technique is applicable only when there are no field inhomogeneities.

In practice, the two image approach requires a static field homogeneity of better than 0.3 ppm to be accurate to within 10%. For example, a 1 ppm inhomogeneity is equivalent to a 60° error in phase, and a fat only region will falsely yield a water and fat reading. These inhomogeneities may be present in the empty magnet or may be the results of the subject's interaction with the static field. The three image technique presented here allows the separation of water, fat and total field inhomogeneity. Adding a fourth experimental measurement, such as a static field plot, allows the separation of water, fat, static field inhomogeneity and subject susceptibility induced inhomogeneity.

[1] P. Margosian and J. Abart, Proc. S.M.R.M., New York, N.Y. 495 (1984).
[2] K.N. Scott and T.H. Mareci, Proc. S.M.R.M., New York, N.Y. 668 (1984.

## MULTIPLE QUANTUM TECHNIQUES IN NMR IMAGING AND SPECTROSCOPY

**Charles L. Dumoulin**

**General Electric Corporate Research and Development Center, PO Box 8, Schenectady, New York 12301**

**Multiple quantum and zero quantum transitions are allowed for any spin system with more than one energy level. Coupled spin 1/2 systems for example, can have spin states in which coherence exists between energy states connected by a multiple quantum transition. These transitions are not directly observable and special pulse sequences are required to detect them. Nevertheless, the unique properties of multiple and zero quantum transitions are particularly attractive. Multiple quantum techniques have been used in high resolution NMR spectroscopy to eluciate and in some cases map out molecular structure. These experiments are instrumentally demanding but for the most part are within the capabilities of modern research grade MR imagers. Water does not exhibit any multiple quantum behavior. Lipids, lactic acid and other metabolites on the other hand can have strong multiple quantum coherence which can be indirectly detected without interference from single quantum water signals. This is possible because of differences in behavior of single and multiple quantum coherence as a function of the phases of the excitation pulses. The traditional vector model inadequately describe multiple quantum behavior and density matrix formalism must be invoked if one is to fully appreciate the complexity and utility of multiple quantum coherence. For example, density matrix calculations predict that the double quantum spectrum of a coupled AB spin 1/2 system will have a single peak at the sum of the chemical shifts of the coupled resonances. The zero quantum spectrum on the other hand will have a single peak at the difference of the chemical shifts of the coupled spins. Zero quantum coherence is particularly interesting since it is independent of magnetic field inhomogeneities. Several spectroscopic and imaging experiments exploiting multiple quantum coherence will be presented.**

## CONTRAST ENHANCEMENT OF MRI IMAGES BY DIGITAL PROCESSING

Schonfeld, E., Evans, H., LeBlanc, A., Schneider, V., Johnson P.

NASA Johnson Space Center and Baylor College of Medicine, Houston, Texas

We have investigated the use of several digital image processing techniques in order to improve image contrast. These techniques have been successfully applied by NASA to remote sensing images from space. Three techniques to improve contrast by feature and edge detection will be presented. These methods are: artificial illumination, 3 color combination classification, and least-squares Laplacian edge detection.

Small intensity variations are very difficult to detect by the eye especially if the image is noisy. A technique that has proven useful for interpreting geographical maps, artificial illumination, may be use-

ful for enhancing image contrast of MRI images. In this technique one computes the reflected light as a result of artificially illuminating a surface. This artificial illumination method uses the directional derivative of the image intensity which gives the illusion of relief in 3 dimensions. It is a natural process to interpret shadows in terms of relief. It also increases the contrast of very small intensity variations in an image. This technique has higher contrast than contoured or pseudo-color images because it contains more intensity levels. To decrease noise, the method uses a special least-squares version of the directional derivative. It was found that the technique was useful for determining the boundaries between muscles, such as the gastrocnemius and soleus.

A technique called three color combination digitally combines the information from 3 different images to produce a single color image. Each of the 3 images is assigned a basic color such as red, green, or blue with the combined image being a mixture of the 3 colors. The final intensity and color is determined by the color intensity of each of the primary images. In MRI one could assign a primary color to images generated by different pulse sequences or MRI parameters such as T1, T2, spin density, blood flow or any other mathematically derived image. Any three of the above can be combined to produce an image with increased information or contrast. This technique was applied to MRI echo images to help differentiate tissues.

It is necessary to accurately determine tissue edges in order to measure size and shape. This is sometimes difficult for small structures such as blood vessels, because of spatial resolution limitations. One way to detect edges is the Laplacian method by Rosenfeld. However, if the data is noisy the noise is amplified because of the differential nature of the method. A least-squares version of the Laplacian was used to decrease the noise to a tolerable level by fitting a paraboloid using least squares to an area typically 5x5 pixels and then computing the Laplacian. This technique was used to detect the edges of limb blood vessels. After the edges were detected the areas and diameters were determined. It was found that this method was more precise than visual edge detection and should lessen interoperator variability.

## MR DIAGNOSIS OF INFERIOR VENA CAVAL ABNORMALITIES

Anthony R. Lupetin, M.D., Nilima Dash, M.D., Rolf L. Schapiro, M.D., Ziad L. Deeb, M.D., Richard H. Daffner, M.D., Robert Sefczek, M.D.;

Allegheny General Hospital, Pittsburgh, Pennsylvania U.S.A.

In a nine-month period, ten patients have undergone evaluation of the inferior vena cava with magnetic resonance. All studies were performed on the **Siemens' Magnetom,** a 0.5 Tesla proton NMR system utilizing a superconductive magnet which is cooled with liquid helium and nitrogen and operates at a nominal field strength of 0.352 Tesla. The radiofrequency system operates at 15 mHz.

MR appears to be the procedure of choice in screening the inferior vena cava for abnormalities. Direct sagittal imaging of the vena cava in most patients can demonstrate the entire intra-abdominal portion of the inferior vena cava.

We will demonstrate cases of inferior vena caval thrombosis, both idiopathic and secondary to renal vein thrombosis extension. We will demonstrate extension of renal carcinoma into the inferior vena cava. We will demonstrate invasion of the inferior vena cava by hepatoma and also by metastatic colon carcinoma in the retroperitoneum.

We will discuss the differentiation of slow flow from tumor or idiopathic thrombus. We will also demonstrate the paradoxical enhancement seen on the first slice when the inferior vena cava is being studied with magnetic resonance.

## GATED CARDIAC IMAGING USING A 0.3 TESLA PERMANENT MAGNET IMAGING SYSTEM

Antoinette S. Gomes, M.D., Juan F. Lois, M.D., Larry-Stuart Deutsch, M.D.

UCLA School of Medicine, Center for the Health Sciences, Department of Radiology, Los Angeles, CA 90024

The purpose of this study is to evaluate the utility of NMR imaging using a 0.3 Tesla whole body permanent magnet imaging system. Thus far 6 normal and 28 abnormal patients with known cardiac disease have been studied. All abnormal patients have had clinical examination, echocardiography, and angiography and in some instances a PET scan. Patients with a spectrum of lesions including hypertrophic cardiomyopathy (8), cardiac tumors (2), coronary artery disease (6), coronary artery bypass grafts (6), and congenital heart disease (6) have been imaged. All images have been acquired with ECG gating using spin echo technique.

Coronary artery grafts have been imaged. Early results with simple oblique and orthogonal views are promising. Native coronary arteries are more difficult to evaluate because of their complex course. Surface coils have been applied in several instances in an attempt to improve coronary artery visualization with varying results. Additional experience is needed to evaluate the usefulness of NMR in coronary artery imaging. Cardiac tumors were well visualized and their relationship to mediastinal structures could be assessed in both cases. In our experience NMR is found to be particularly useful in

evaluating results of radiation and chemotherapy. In hypertrophic cardiomyopathy there was clear visualization of the interventricular septum and the ventricular chambers. In complex congenital heart disease NMR is particularly useful for evaluation of post-operative results as good visualization of all chambers was obtained. Larger numbers of patients, however, are needed to ascertain the sensitivity and accuracy of NMR in the detection of small inter-atrial and inter-ventricular septal defects.

## REDUCTION OF MOTION ARTIFACTS IN NMR IMAGING

R.E. Gangarosa, A.V. Lakshminarayanan, S. Albert, P. Coleman, D. Frizzell, J. Hahn, C. Huebner, M. Profeta, P. Pattany

Picker International, 5500 Avion Park Drive, Highland Heights, Ohio 44143

Movement artifact represents one of the most severe problems limiting clinical effectiveness of NMR imaging, especially in the thorax and abdomen. Types of motion artifact analyzed here include cardiac, respiratory, peristaltic and blood flow movement. The aim of this paper is to investigate characteristics of motion artifact and to determine practical methods to reduce them.

Since each NMR acquisition occurs rapidly compared to physiological movement, most movement artifact results from view-to-view variation in image data registration. Thus, the appearance of motion artifacts depends on the relationship between the characteristics of the motions (i.e., type, regularity, period, amplitude, etc.), the observational parameters (i.e., pulse sequence, coil, field strength, slice orientation, etc.), and the reconstruction technique (2DFT, projection reconstruction, hybrid).

The images were obtained with Picker International Vista™ MR imagers operating at fields of 0.15, 0.5, 1.0 and 1.5T. Our experiments suggest that the most important imaging parameters influencing this artifact include the choice of TR relative to the movement, choice of pulse sequence, anatomical region and image plane, physiological (cardiac and/or respiratory) gating, choice of spatial encoding techniques and magnetic field strength. The influence of these factors will be demonstrated in clinical and volunteer images.

Analysis of these factors leads to specific maneuvers to reduce movement artifacts. These maneuvers can be categorized as (1) avoiding movement artifacts, (2) suppressing movement, (3) synchronizing data acquisition to movement periodicity, (4) reducing the influence of movement on the signal and (5) diffusing the movement artifact. Examples of maneuvers which fall into the five categories listed above are (1) choice of coronal scans in abdominal imaging, (2) use of glucagon in suppressing peristalsis, (3) use of cardiac and/or respiratory gating, (4) use of a pulse sequence adaptation which reduces flow artifacts, and (5) use of hybrid complex modulation or back projection with 2-sided echo sampling and magnitude reconstruction. These maneuvers can be used singly or in combination. Example images will be shown to demonstrate the effects of these maneuvers. Using these maneuvers, all types of movement artifacts considered could be minimized.

## EFFECTIVE ENCODING STRATEGIES FOR MRI: A TWO-ECHO FLOW/MOTION AND CHEMICAL SHIFT SEQUENCE WITH STEREO-VIEWS

Paul R. Moran, Bowman Gray School of Medicine
William H. Perman, University of Wisconsin
Richard A. Moran, General Electric Medical Systems

A number of effective strategies for multiple encoded MRI scans can be designed. An example is a two-echo sequence in which the second echo is coded for multiple sampling of phase-gradient-modulation true flow/motion imaging, and the first echo-data are coded for chemical shift imaging (e.g., to extract separate fat/water information). We have implemented this sequence on two different scanners, one at 1.5T and one at 0.15T, and have demonstrated successful performance on both. We also have demonstrated the possibility of carrying out the scan in full-projection imaging mode in coronal view on both instruments. It also is a characteristic of this type of sequence that ordinary conventional MR-images can be reconstructed from the same raw-data, as well as the true flow-images and the fat/water discriminated images. We demonstrate the results of this feature.

By adding a repeat of the same sequence, i.e., doubling the "average-chop," and modifying the read-out gradient command to activate a simultaneous weak gradient along the direction of the imaged plane, we can achieve even further capability. In this extended mode, we carry out a "thick slab" selective excitation and obtain parallax stereo-views in the reconstructed image. These may be viewed through a binocular viewer to produce, for example, a three-dimensional presentation of the vascular flow in the imaged slab.

## THREE DIMENSIONAL N.M.R. IMAGING

By R.A. Jones

Dept. of Bio-Medical Physics, University of Aberdeen, Scotland.

Three dimensional N.M.R. images have been obtained using 3D spin-warp (3DSW) and 3D recalled echo (3DRE) techniques. Full details of the pulse sequences can be found in reference 1.

For both techniques the field of view and spatial resolution in each of the three orthogonal directions are independant, allowing the imaging volume to be tailored, to some extent, to the volume of interest. Slice selection is achieved by using an optimised sinc (2) for the R.F. envelope and a suitable selection gradient. The encoded region is made slightly larger than the selected region to rule out the possibility of aliasing in the slice direction. This combined with the fall off in signal at the edges of the selected region means that the slices at either extreme will have a degraded signal to noise ratio (SNR). An image resolution of 64x64x8 has been implemented for both techniques, a 128x128x8 matrix has been implemented only for the 3DSW method. Data processing for the two techniques is identical providing only the alternate echoes from the 3DRE sequence are sampled. If all of the echoes produced by the 3DRE sequence are to be processed then the 'even' (time reversed) echoes require additional processing. Because the collection time is limited by $\Delta B_o$ and $T_2$ effects it is necessary to use a higher signal bandwidth for the 3DRE since it will be necessary to recall and sample the free induction signal (FIS) 8 times for a resolution of 8 in the slice direction.

The 3DSW technique gives an improvement of $\sqrt{N}$, where N is the number of planes, over a 2D spin-warp image of the same plane with the same voxel dimensions. If the collection time following a single FIS is the same for the 3DRE and 2D methods and only alternate echoes are collected in the former then the signal bandwidth must increase by a factor of 16 for the 3DRE method. This will increase the noise by a factor of 4, however as 8 echoes are sampled the overall reduction in SNR is only $\sqrt{2}$, this reduction occurs as only alternate echoes are being collected. Collecting all of the echoes will produce an SNR equivalent to that of the 2D method, in practice the time required for gradient switching wii degrade the SNR of the 3DRE method. These results have been confirmed experimentally, with the SNR of the 3DRE method being better than indicated above due to it having a longer collection time per FIS than the 2D technique. The penalty for the high SNR of the 3DSW method is it's relatively long acquisition time. This can be reduced by using a short inter-pulse interval, at our operating frequency of 1.7MHz this also serves to increase the contras in the images. The 3DRE technique has the advantage of a short acquisition time and should prove useful in applications where it is necessary to use a longer interpulse interval, e.g. in 3D gated cardiac images.

References

1 G.Johnson,J.M.S.Hutchison,T.W.Redpath and L.M.Eastwood - J. Magn. Reson. 54,374-384 (1983)

2 D.J.Lurie - Magn. Reson. Imaging, submitted

## MECHANICAL SHIMMING OF RESISTIVE OR SUPERCONDUCTIVE MAGNETS FOR MAGNETIC RESONANCE IMAGING

Hervé SAINT-JALMES - Institut d'Electronique Fondamentale Bâtiment 220 91405 Orsay Cedex (F)
Yves BARJHOUX - Thomson CGR, B.P. 34 78530 Buc (F)

High homogeneity magnets for NMR require some means of shimming. This is first done at assembly time, before and after cooling in the case of a superconductive magnet. It is then repeated on the installation site. One should compensate for i) manufacturing and assembly tolerances and ii) environmental field distorsions. Shimming can be achieved by mechanical realignment of the magnet elements, by electrical adjustments or by local compensations with magnetic materials. When the magnet structure allows it, mechanical shimming is most effective for problem i) and presents significant advantages for problem ii), although electrical shims will eventually be used as a final refinement.

The various procedures for mechanical shimming of a large magnet are compared through the successive steps of field homogeneity measurements, characterization of the field defects by their symetry features and the crucial choice of a corrective action among many. The mathematical analysis of all elementary realignments is done with simulated field plots (see figure).

Several procedures have been used for alignment of three different resistive magnets for whole body MRI. The new procedure we propose relies on characterization of the symetry and quantitative assessment of the amplitude of each field defect of the whole magnet. It has proven vastly superior and much quicker than the conventional methods based either on successive single coil alignments or on partial derivatives estimation for each action.

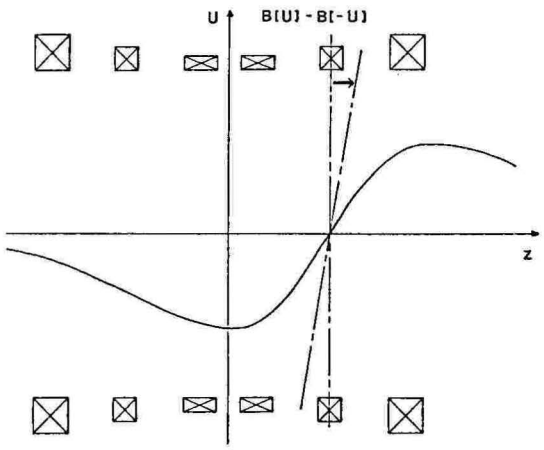


Figure 1 :

Simulated field plot of an elementary misalignment.
Each coil has five degrees of freedom, one axial, two radial and two rotational.
The effect along the Z-axis of a rotational error is shown.

**MAGNETIC SHIELDS FOR MR MAGNETS**

A.K. Kalafala (Ph.D) R.M. Vavrek*

General Electric Corporate Research and Development
* General Electric Medical Systems Business Group

Siting of an MR magnet in any environment, such as a hospital, requires consideration of several factors:

- o Minimizing the effect of the stray magnetic field on the surrounding equipment and personnel.
- o Minimizing the effect of the surrounding structural environment on the field homogeneity within the magnet's working volume.
- o Minimize the additional installation cost due to any proposed shielding configuration.

Presently, work is in progress on the design of ferromagnetic shields to meet the above requirements. Extensive use is made of the family of linear and non-linear Electromagnetic Analysis Codes developed in house to aid in optimizing shield configurations.

Shield Geometry - Geometrical symmetry with respect to the magnet axis is usually the starting point. A cylinder, due to its symmetry, causes minimum perturbation to the field homogeneity in the working volume. On the other hand, box like shields and planar flat parallel shields may be more appropriate where selective shielding of certain areas is meets hospital requirements.

Shield Material - Optimum shielding capability calls for the selection of materials with the highest level of magnetization at the prevailing fields which may vary from a high of 3000 gauss at the magnet surface to a low of 1 gauss in the magnet fringe field.

Shield Location - In one extreme case the shield is integrated with the magnet in a "self-shielded" design which is site independent. In the other extreme case the magnetic material is located on a suitable wall and can be asymmetric. Site requirements and restrictions ultimately dictate the location and shape of the magnetic shield.

An example is given of a self-shielded 1.5T MR magnet under construction. The shield is close to the magnet forming an axi-symmetric structure weighing 21 tons. A second example is given of a room shield which has been built for the San Francisco CMR. The room shield weighs 57 tons and meets more stringent stray field requirements than first shield.

SITING OF NONSUPERCONDUCTIVE MRI SYSTEMS

Richard Genberg and John Cassesse

Fonar Corporation, 110 Marcus Drive, Melville, NY 11747

To date many papers have been presented on the siting requirements of superconductive MRI systems. In such installations one must consider the large fringe fields, intolerance to ferrous materials in their environment, the necessity for the storage of cryogens, the need for large areas to isolate the system or even the construction of a separate building.

In comparison, the installation of nonsuperconductive MRI scanners avoids most of these complexities. Nonsuperconductive MRI scanners of the Fonar design have negligible fringe field. This one feature allows this type of system the freedom to be installed almost anywhere, with the permanent magnet system requiring less than 1000 square feet.

Supporting the weight of the magnet is the only special consideration necessary when selecting a site.

For a ground floor installation 12 inches of concrete are all that is required to install the system. On a first floor installation or higher a weight distribution system must be considered and must be designed for each location. The permanent magnet is assembled on site making extensive renovation of existing facilities unnecessary. Due to a lack of fringe field ordinary structural steel can be used keeping the costs down. A typical first floor installation would cost approximately $50,000-75,000. Siting requirements for installation of nonsuperconductive MRI scanners will be discussed in detail.

## MOBILE MAGNETS FOR MAGNETIC RESONANCE IMAGING

W.D. Markiewicz, F.S. Murray, P.A. Jonas, T.R. Farnum, R.F. DiGesare, R.E. Wilcox, C.L. Linkinhoker

Intermagnetics General Corporation, Guilderland, NY

It now appears that mobile magnetic resonance imaging units will find an important place in the total installed MRI capacity. The reasons for this include the expense of fixed site installations and the desirability to remain flexible in the early developments of a major new technology. Initial mobile units have been introduced for evaluation and service. It is appropriate to review the design requirements imposed on the MRI magnet system in the mobile configuration and to indicate how the mechanical, electrical and cryogenic issues have been addressed. A typical magnet operation sequence is described. Possibilities for the future direction of refrigeration and magnetic field shielding are indicated. Finally, available initial experience with the mobile MRI magnets in service will be reported.

## FRINGE MAGNETIC INDUCTION FOR 0.5T SUPERCONDUCTING MRI IN A MAGNETICALLY SCREENED SITE.

D.W. Anderson, W.S. Yamanashi and P.D. Lester
Department of Diagnostic Imaging and Radiation Medicine, City of Faith Medical and Research Center, Tulsa, OK 74137-1270

Algebraic experessions for the magnetic induction in the fringe area around a solenoidal MRI magnet were developed for the nonscreened case in the magnetic dipole approximation.

$$B_z = \frac{B_o Z_e^2}{4}\left\{\frac{Z - Z_e}{[R^2 + (Z - Z_e)^2]^{3/2}} - \frac{Z + Z_e}{[R^2 + (Z + Z_e)^2]^{3/2}}\right\}, B_r = \frac{B_o Z_e^2}{4}\left\{\frac{R}{[R^2 + (Z - Z_e)^2]^{3/2}} - \frac{R}{[R^2 + (Z + Z_e)^2]^{3/2}}\right\}$$

In this case Z is the axial coordinate, $Z_e$ is the magnet half length, R is the coordinate perpendicular to the axis and $B_o$ is the magnetic induction in the bore. Their expressions give results which agree well with values on the isogauss contour paps given by the magnet manufactures[1] and shown by other researchers[2] as long as $Z \gg Z_e$ and $R \gg Z_e$. To evaluate the effect of the screening (5/8" steel plate) used on the sidewalls, ceiling and under the floor, the fringe magnetic induction was carefully measured and results compared with the non-screened values obtained using the above equations. The effect of the screening was to move the 10 gauss line and the 5 gauss line appreciably closer to the magnet at the lateral sides. This saving in space is significant when a previously constructed site in a functioning radiology department is adopted for MRI. Practical safety consideration at 0.5T central field in this particular setting has been reported[3].

[1] Oxford Magnet Technology, Magnets in Clinical Use, Onsney Mead, Oxford OX20DX, 1983.

[2] H. Mano, Fringe Magnetic Fields at 0.15, 0.2 and 0.5T for Hospital MRI, Absr. 3rd Annual Meeting. Society of Magnetic Resonance in Medicine, August 13-17, New York, 1984, pp. 490-491.

[3] D.W. Anderson, W.S. Yamanashi, et al, Fringe Magnetic Field Survey of a Hospital MRI Site at 0.5 Central Field. Abstr. 3rd Annual Meeting. Society of Magnetic Resonance in Medicine, August 13-17, 1984, pp. 5,6.